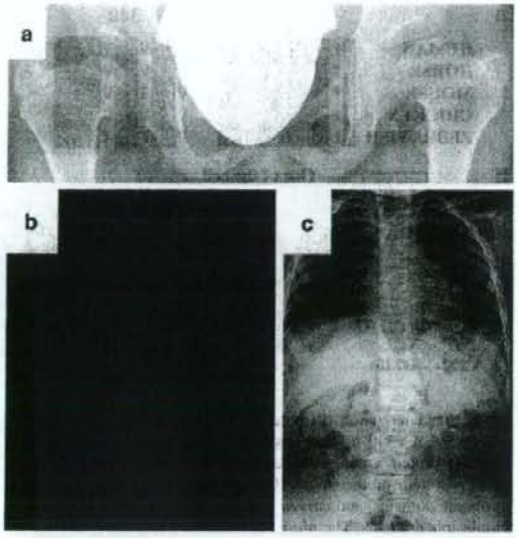

Fig. 2 X-rays at 4 years of age. **a** Bilateral hip joints had acetabular dysplasia. Femoral heads were slightly flat and femoral necks were broad. As a result, coxa vara was displayed. **b** Carpal bone ossification was advanced; seven carpal bones were visible in this 4-year-old hand. **c** Total spine showed mild scoliosis and mild flattening of vertebrae

Detection of mutations

Peripheral blood samples of the patient, her parents, and 96 unrelated normal Japanese controls were obtained with written informed consent. Genomic deoxyribonucleic acid (DNA) samples were extracted by standard procedures. The entire coding region and flanking intronic regions were examined by polymerase chain reaction (PCR) and direct sequence analysis (Ikeda et al. 2001). Direct sequencing was performed using an ABI prism 3700 automated sequencer (Applied Biosystems, Foster City, CA, USA). To obtain allelic information, PCR products containing mutations were cloned using a TOPO TA cloning kit (Invitrogen, Carlsbad, CA, USA) and sequenced. The paternity was confirmed by ten unlinked microsatellite markers. They were genotyped using an ABI prism linkage mapping set v2.5 and an ABI prism 3700 automated sequencer (Applied Biosystems) by standard procedures.

Evaluation of mutations

To investigate the conservation of mutated amino acids p.T266 and p.V340, reference sequences of human (NP_000103), horse (NP_001075403), mouse (NP_031911), chicken (XP_425183), and zebra fish (XP_685114) were obtained from the National Center for Biotechnology Information (http://www.ncbi.nlm.nih.gov/). PSORT, a computer program for the prediction of protein localization sites in cells (http://psort.nibb.ac.jp/), was used to predict the structure before and after introduction of p.T266I.

Table 1 A summary of mutations in this case

Nucleotide	Amino acid	dbSNP No	AF	Mutation DB
c.797C > T	p.T266I	(–)	(–)	(–)
c.1018–1020del	p.ΔV340	(–)	(–)	ACG1B, DTD
c.2065A > T	p.T689S	rs3776070	0.167	Polymorphism

p.ΔV340: a common mutation reported as null mutation (Karniski 2004)

ACG1B achondrogenesis 1B, *DTD* diastrophic dysplasia, *AF* allele frequency, (–) no data in database

Results

Detection of mutations

The entire coding region and flanking intronic regions of *DTDST* were directly sequenced. Two heterozygous mutations, c.797C > T (p.T266I) and c.1018-1020del (p.ΔV340), were detected (Table 1). The former was not found in the public database for single nucleotide polymorphism (SNP) and mutation or in 96 unrelated Japanese controls, whereas the latter was recurrent (Superti-Furga et al. 1996b). Polymerase chain reaction (PCR) products containing two mutations were cloned to obtain allelic information, and the patient was recognized as a compound heterozygote of the two mutations (Fig. 3a). The two mutations were searched in the parents by direct sequence. A heterozygous mutation of c.1018-1020del (p.ΔV340) was recognized in the mother, but neither of the mutations was found in the father (Fig. 3b). Paternity was confirmed by genotyping unlinked ten microsatellite markers for the patient and parents.

Evaluation of mutations

Amino acid sequences of DTDST were compared between five diverse species; p.T266 and p.V340 were conserved in all five species (Fig. 4a). Using PSORT, the structural change of DTDST protein was predicted. T266 was outside of the cell, but I266 was in the plasma membrane. The introduction of p.T266I caused ten-amino-acids shortening of the third cytoplasmic domain and ten-amino-acids elongation of the third extracellular domain of the DTDST protein (Fig. 4b).

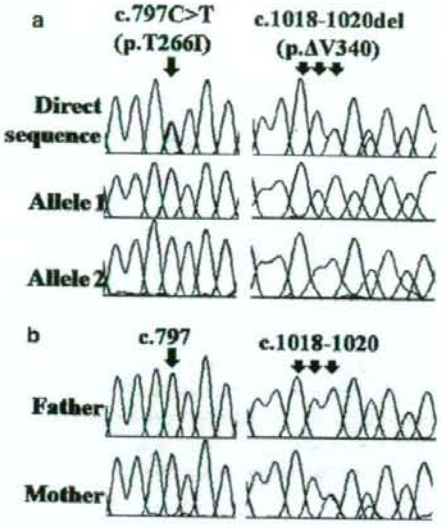

Fig. 3 a Sequences of the patient. *Top* direct sequence; *middle and bottom* sequences after TA cloning. The *red*, *blue*, *green*, and *black waves* represent nucleotides, thymine, cytosine, and adenine and guanine, respectively. The patient had heterozygous *DTDST* mutations, c.797C > T (p.T266I) and c.1018-1020del (p.ΔV340). **b** Direct sequences of the parents. The mother was a heterozygote of c.1018-1020del (p.ΔV340), but the father had neither of these two mutations

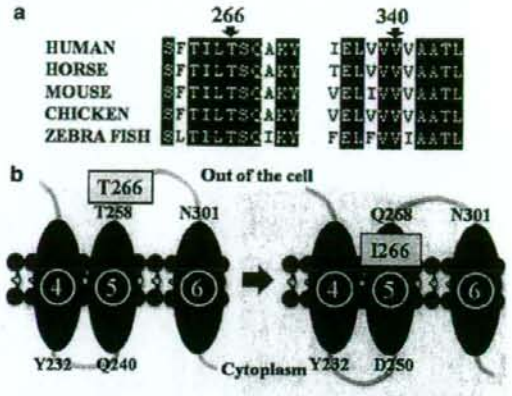

Fig. 4 Characterization of mutated amino acids. a Conservation of p.T266 and p.V340 in the diastrophic dysplasia sulfate transporter (DTDST) protein among different species. b Structural change of a DTDST protein predicted by PSORT. *Ellipses* represent the transmembrane domains, and *curved lines* represent either extracellular or cytoplasmic domains. The *plain numbers* are neighboring amino acid numbers of transmembrane domains shown at those positions. The *circled numbers* are transmembrane domain numbers from the N-terminus. If a 266th amino acid (*squared*) changed from threonine (*T*) to isoleucine (*I*), it would migrate from outside of the cell into the plasma membrane. The length of the fifth transmembrane domain would not change, but that of the neighboring third extracellular and third cytoplasmic domain would be shortened and elongated by ten amino acids, respectively

Discussion

r-MED and DTD are milder diseases in the DTD group. r-MED patients are not short, and they are healthy in childhood other than occasional associations with clubfeet and cleft palate. The radiological hallmarks include, as in the child in this study, broad proximal femora with proximal femoral epiphyseal dysplasia and undertubulated short tubular bones. By contrast, DTD presents with pre- and postnatal short stature, distinctive hitchhiker thumbs, inflammatory ear swelling, and intractable clubfeet, as well as joint dislocations and spinal malalignment. The skeletal changes are variable among affected individuals. Broad proximal femora and undertubulated short tubular bones are occasional, but not exclusive, findings. The presence of short stature and the radiological constellation of the child reported here fit an intermediate between r-MED and DTD.

Of note is that in this case, skeletal changes in infancy were reminiscent of Desbuquois dysplasia. r-MED and DTD also show broad proximal femora with prominence of the lesser trochanters, but those are not so prominent that are comparable to Swedish-key appearance. Mildly advanced carpal and tarsal ossifications are known in DTD but are not so prominent as those in this case or Desbuquois dysplasia.

c.1018-1020del (p.ΔV340) is a relatively common mutation in DTD and ACG-1B. Immunofluorescence analysis showed that p.ΔV340 was not on the plasma membrane, although DTDST was a plasma membrane protein. Therefore, it was classified as a null mutation and associated with severe phenotypes of the DTD group (Karniski 2004). c.797C > T (p.T266I) is a novel mutation, which is supported by its de novo occurrence during paternal gametogenesis. Conservation between diverse species suggests that p.T266 plays an important role in DTDST protein. T266 was predicted to be outside of the plasma membrane because of its OH base, which had no affinity to lipid but to H_2O. On the other hand, I266 was predicted to migrate in the plasma membrane because it had nonpolarity and high affinity to lipid. As a consequence, the structure of DTDST protein would change drastically, most likely affecting its sulfate transport function.

According to a previous report (Karniski 2004), nonlethal disorders caused by *DTDST* mutations would be either a heterozygote of partial-function mutation and null mutation or a homozygote of partial-function mutations. The phenotypes of the child in this study fell into the milder range of the DTD group, and she had p.ΔV340, a null mutation. Therefore, it seems that c.797C > T (p.T266I) is classifiable as partial-function mutation, the sulfate transport activity of which is only mildly affected

and in which localization is predicted to be on the plasma membrane. The result of the PSORT analysis supports this presumption. Further functional evidence is needed to validate the mutation function.

Thus, we first report a novel *DTDST* mutation, p.T266I, that results in a novel phenotype in combination with a recurrent null mutation, further extending the phenotypic spectrum of *DTDST* mutations. We hope that these findings will support clinical and genetic diagnosis of similar chondrodysplasias.

Acknowledgments We thank the patient and her parents for cooperation in the study. This work was supported by grant-in-aid from Development of New Approach for Regenerative Medicine.

References

Faivre L, Cormier-Daire V, Younf I, Bracq H, Finidori G, Padovani JP, Odent S, Lachman R, Munnich A, Maroteaux P, Le Merrer M (2004) Long-term outcome in Desbuquois dysplasia: a follow-up in four adult patients. Am J Med Genet A 124:54–59

Hall CM (2002) International nosology and classification of constitutional disorders of bone (2001). Am J Med Genet 113:65–77

Hastbacka J, de la Chapelle A, Mahtani MM, Clines G, Reeve-Daly MP, Daly M, Hamilton BA, Kusumi K, Trivedi B, Weaver A, Coloma A, Lovett M, Buckler A, Kaitila I, Lander ES (1994) The diastrophic dysplasia gene encodes a novel sulfate transporter: positional cloning by fine-structure linkage disequilibrium mapping. Cell 78:1073–1087

Hastbacka J, Superti-Furga A, Wilcox WR, Rimoin DL, Cohn DH, Lander ES (1996) Atelosteogenesis type II is caused by mutations in the diastrophic dysplasia sulfate-transporter gene (DTDST): evidence for a phenotypic series involving three chondrodysplasias. Am J Hum Genet 58:255–262

Ikeda T, Mabuchi A, Fukuda A, Hiraoka H, Kawakami A, Yamamoto S, Machida H, Takatori Y, Kawaguchi H, Nakamura K, Ikegawa S (2001) Identification of sequence polymorphisms in two sulfation-related genes, PAPSS2 and SLC26A2, and an association analysis with knee osteoarthritis. J Hum Genet 46:538–543

Karniski LP (2001) Mutations in the diastrophic dysplasia sulfate transporter (DTDST) gene: correlation between sulfate transport activity and chondrodysplasia phenotype. Hum Mol Genet 10:1485–1490

Karniski LP (2004) Functional expression and cellular distribution of diastrophic dysplasia sulfate transporter (DTDST) gene mutations in HEK cells. Hum Mol Genet 13:2165–2171

Lachman RS (1998) International nomenclature and classification of the osteochondrodysplasias (1997). Pediatr Radiol 28:737–744

Maeda K, Miyamoto Y, Sawaki H, Karniski LP, Nakashima E, Nishimura G, Ikegawa S (2006) A compound heterozygote harboring novel and recurrent *DTDST* mutations with intermediate phenotype between Atelosteogenesis type II and Diastrophic dysplasia. Am J Med Genet A 140:1143–1147

Mégarbané A, Haddad FA, Haddad-Zebouni S, Achram M, Eich G, Le Merrer M, Superti-Furga A (1999) Homozygosity for a novel DTDST mutation in a child with a 'broad bone-platyspondylic' variant of diastrophic dysplasia. Clin Genet 56:71–76

Nishimura G, Hong HS, Kawame H, Sato S, Cai G, Ozono K (1999) A mild variant of Desbuquois dysplasia. Eur J Pediatr 158:479–483

Rossi A, Superti-Furga A (2001) Mutations in the diastrophic dysplasia sulfate transporter (DTDST) gene (SLC26A2): 22 novel mutations, mutation review, associated skeletal phenotypes, and diagnostic relevance. Hum Mutat 17:159–171

Rossi A, Bonaventure J, Delezoide AL, Superti-Furga A, Cetta G (1997) Undersulfation of cartilage proteoglycans ex vivo and increased contribution of amino acid sulfur to sulfation in vitro in McAlister dysplasia/atelosteogenesis type 2. Eur J Biochem 248:741–747

Rossi A, Kaitila I, Wilcox WR, Rimoin DL, Steinmann B, Cetta G, Superti-Furga A (1998) Proteoglycan sulfation in cartilage and cell cultures from patients with sulfate transporter chondrodysplasias: relationship to clinical severity and indication on the role of intracellular sulfate production. Matrix Biol 17:361–369

Superti-Furga A, Hastbacka J, Wilcox WR, Cohn DH, van der Harten HJ, Rossi A, Blau N, Rimoin DL, Steinmann B, Lander ES, Gitzelmann R (1996a) Achondrogenesis type IB is caused by mutations in the diastrophic dysplasia sulphate transporter gene. Nat Genet 12:100–102

Superti-Furga A, Rossi A, Steinmann B, Gitzelmann R (1996b) A chondrodysplasia family produced by mutations in the diastrophic dysplasia sulfate transporter gene: genotype/phenotype correlations. Am J Med Genet 63:144–147

Superti-Furga A, Neumann L, Riebel T, Eich G, Steinmann B, Spranger J, Kunze J (1999) Recessively inherited multiple epiphyseal dysplasia with normal stature, club foot, and double layered patella caused by a DTDST mutation. J Med Genet 36:621–624

Superti-Furga A, Unger S, the Nosology group of the international skeletal dysplasia society (2007) Nosology and classification of genetic skeletal disorders: 2006 revision. Am J Med Genet A 143:1–18

Cell Stem Cell
Article

Ontogeny and Multipotency of Neural Crest-Derived Stem Cells in Mouse Bone Marrow, Dorsal Root Ganglia, and Whisker Pad

Narihito Nagoshi,[1,2] Shinsuke Shibata,[1] Yoshiaki Kubota,[3] Masaya Nakamura,[2] Yasuo Nagai,[1] Etsuko Satoh,[1] Satoru Morikawa,[1,4] Yohei Okada,[1,6] Yo Mabuchi,[1] Hiroyuki Katoh,[2] Seiji Okada,[1,7] Keiichi Fukuda,[5] Toshio Suda,[3] Yumi Matsuzaki,[1] Yoshiaki Toyama,[2] and Hideyuki Okano[1,*]
[1]Department of Physiology
[2]Department of Orthopedic Surgery
[3]Department of Cell Differentiation
[4]Department of Dentistry and Oral Surgery
[5]Department of Regenerative Medicine and Advanced Cardiac Therapeutics
Keio University School of Medicine, 35 Shinanomachi, Shinjuku-ku, Tokyo 160-8582, Japan
[6]Department of Neurology, Nagoya University Graduate School of Medicine, 65 Tsurumai-cho, Showa-ku, Nagoya 466-8550, Japan
[7]SSP Stem Cell Unit, Graduate School of Medical Science, Kyushu University, 3-1-1 Maidashi, Higashi-ku, Fukuoka 812-8582, Japan
*Correspondence: hidokano@sc.itc.keio.ac.jp
DOI 10.1016/j.stem.2008.03.005

SUMMARY

Although recent reports have described multipotent, self-renewing, neural crest-derived stem cells (NCSCs), the NCSCs in various adult rodent tissues have not been well characterized or compared. Here we identified NCSCs in the bone marrow (BM), dorsal root ganglia, and whisker pad and prospectively isolated them from adult transgenic mice encoding neural crest-specific P0-Cre/Floxed-EGFP and Wnt1-Cre/Floxed-EGFP. Cultured EGFP-positive cells formed neurosphere-like structures that expressed NCSC genes and could differentiate into neurons, glial cells, and myofibroblasts, but the frequency of the cell types was tissue source dependent. Interestingly, we observed NCSCs in the aorta-gonad-mesonephros region, circulating blood, and liver at the embryonic stage, suggesting that NCSCs migrate through the bloodstream to the BM and providing an explanation for how neural cells are generated from the BM. The identification of NCSCs in accessible adult tissue provides a new potential source for autologous cell therapy after nerve injury or disease.

INTRODUCTION

The neural crest is a transient embryonic tissue that originates at the neural folds during vertebrate development. Neural crest cells delaminate from the dorsal neural tube and migrate to various locations, where they differentiate into a vast range of cells, including neurons and glial cells of the autonomic and enteric nervous systems, smooth muscle cells of the heart and great vessels, and bone and cartilage cells of the face (Le Douarin and Kalcheim, 1999).

From the embryonic period through adulthood, neural crest cells are generated by neural crest-derived stem cells (NCSCs), which are self-renewing and multipotent, with the potential to differentiate into neurons, glial cells, and myofibroblasts (Morrison et al., 1999; Shah et al., 1996). NCSCs have been isolated from the embryonic sciatic nerve (Morrison et al., 1999) and boundary cap (BC) (Hjerling-Leffler et al., 2005) and the gut (Kruger et al., 2002), skin (Fernandes et al., 2004; Sieber-Blum et al., 2004; Wong et al., 2006), heart (Tomita et al., 2005), and cornea (Yoshida et al., 2006) of adult rodents. These reports demonstrate the presence of NCSCs in these tissues and suggest their existence in other adult tissues.

Several types of stem cells have been identified in adult tissues. For example, several groups have described multipotent stem cells in the bone marrow (BM), but the developmental origin and differentiation potential of these cells are unknown (D'Ippolito et al., 2004; Jiang et al., 2002; Ross et al., 2006). These stem cells are reported to generate neural cells and smooth muscle cells, which are known to originate from neural crest cells. Such observations led us to investigate whether some newly identified stem cells might be NCSCs. We examined this hypothesis by investigating various tissues of double-transgenic mice encoding Protein-0 (P0) and Wnt1 promoter-Cre/Floxed-EGFP, in which neural crest-derived cells express EGFP (Danielian et al., 1998; Kawamoto et al., 2000; Yamauchi et al., 1999).

Here, we prospectively isolated and compared neural crest-derived stem and progenitor cells from the BM of the lower extremities, dorsal root ganglia (DRG), and whisker pad (WP) of adult P0 and Wnt1 promoter-Cre/Floxed-EGFP mice. This is the first report identifying NCSCs in the BM of adult rodents. The existence of NCSCs was confirmed in all three tissues, and distinct differences among the NCSCs were revealed by comparing their proliferation capacity, differentiation potential, and gene expression profiles.

RESULTS

Distribution of EGFP-Positive Neural Crest-Lineage Cells in Embryonic and Adult P0 and Wnt1-Cre/Floxed-EGFP Mice

To examine the distribution of neural crest-derived cells in various tissues, we performed histological analyses of

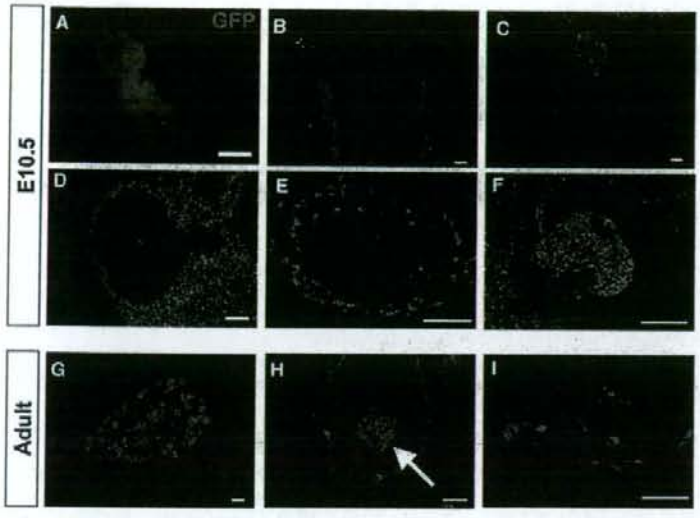

Figure 1. Expression Pattern of EGFP in P0-Cre/Floxed-EGFP Mice at E10.5 and the Adult Stage

(A) Whole-body observation of direct EGFP fluorescence in E10.5 mice.

(B–F) Anti-GFP immunostaining of E10.5 mice revealed EGFP$^+$ cells in the DRG (B), outflow tract of the heart (C), optic mesenchyme (D), gut (E), and trigeminal ganglion (F).

(G–I) In 8-week-old adult mice, EGFP$^+$ cells were detected in the DRG (G), dermal papilla in the whisker follicle (arrow in [H]), and BM of the tibia (I). Scale bars, 1 mm in (A) and 50 μm in (B)–(I).

P0-Cre/Floxed-EGFP mouse embryos and adults. P0 was originally identified as a Schwann cell-specific myelin protein (Lemke et al., 1988), but it is also expressed by migrating neural crest cells during the early embryonic period in chicks (Bhattacharyya et al., 1991). In this transgenic mouse, the transient activation of the P0 promoter induces Cre-mediated recombination, indelibly tagging neural crest-derived cells with EGFP expression (Kawamoto et al., 2000; Yamauchi et al., 1999). At E10.5, EGFP was observed in the pharyngeal arches, periocular region, and front nasal region, which contain neural crest-derived cells (Figure 1A) (Yamauchi et al., 1999). Anti-GFP immunostaining of E10.5 embryos revealed EGFP-positive (EGFP$^+$) cells in the DRG, outflow tract of the aorta, optic mesenchyme, gut, and trigeminal ganglia (Figures 1B–1F). In adult mice, EGFP$^+$ cells were observed in the DRG, dermal papilla of whisker follicles, and BM of the tibia (Figures 1G–1I). As a negative control, we examined anti-GFP staining in single transgenic P0-Cre mice without the Floxed-EGFP reporter and detected no EGFP$^+$ cells (data not shown), confirming the validity of the anti-GFP staining. Immunohistochemistry was also performed on various tissues from adult Wnt1-Cre/Floxed-EGFP mice, confirming the presence of EGFP$^+$ cells in the DRG, dermal papilla, and BM (see Figure S1 available online). These observations suggest that EGFP$^+$ neural crest-derived cells migrate to and survive in various adult tissues.

Since neural crest-derived cells have not been previously reported in the BM, we analyzed the distribution of EGFP$^+$ cells in the BM of P0-Cre/Floxed-EGFP mice by immunohistochemistry. It is unlikely that EGFP expression was induced by the ectopic expression of P0, since we did not detect P0 protein in the BM (Figure S2). In the BM of P0-Cre/Floxed-EGFP mice, EGFP$^+$ cells were detected along blood vessels, especially the vasculature located near the inner surface of the bone cortex (Figures 2A–2C). In whole-mount specimens, these EGFP$^+$ cells were positive for both PECAM-1 and SMA, markers for endothelial cells and smooth muscle cells (Figures 2E–2L), and quantitative analysis revealed that 3.85% and 6.23% of the EGFP$^+$ cells in the BM were positive for PECAM-1 and SMA, respectively. The contribution of EGFP$^+$ cells to the vascular endothelial structure was also confirmed by flow-cytometric analysis (Figure 2D) and whole-mount immunohistochemistry with other vascular markers (Figures 2M–2X). Although a portion of vascular smooth muscle cells are known to be derived from the neural crest, neural crest-derived cells have not been reported in the vascular endothelium in previous studies (Etchevers et al., 2001; Joseph et al., 2004). To corroborate our observations, we examined the BM in adult Wnt1-Cre/Floxed-EGFP mice. Although a similar number of EGFP$^+$ cells was observed, the EGFP$^+$ cells did not express endothelial cell or smooth muscle cell markers (Figures S1C and S1D). Thus, our detailed analyses using two lines of transgenic mice demonstrated the presence of neural crest-derived cells in the BM, but their contribution to blood vessel formation remains unclear.

NCSCs Migrate from the Trunk Dorsal Neural Tube to the Aorta-Gonad-Mesonephros Region and Circulate in the Blood during Embryonic Development

To elucidate the migration route of EGFP$^+$ cells from the trunk dorsal neural tube to the BM, we focused on the aorta-gonad-mesonephros (AGM) region in P0 and Wnt1-Cre/Floxed-EGFP mice. During development, the first adult-type hematopoietic stem cells (HSCs) are generated at E10.5 in the AGM region and migrate via the blood stream to the BM in the late embryonic period (Medvinsky and Dzierzak, 1996; Muller et al., 1994). Mesenchymal stem cells (MSCs) are also generated in the AGM region at E11.0, migrate in the blood stream, and are found in the neonatal BM (Mendes et al., 2005). We therefore hypothesized that neural crest-derived cells take a similar route to the BM, migrating from the dorsal neural tube to the AGM region, from which they then travel through the blood stream to the BM. Anti-GFP immunostaining revealed EGFP$^+$ cells migrating from the trunk dorsal neural tube to the AGM region in E11.0 P0-Cre/Floxed-EGFP mice (Figure 3A). These EGFP$^+$ cells were 100% positive for p75 and 50.6% positive for Sox10, both known as NCSC markers (Paratore et al., 2001; Stemple and Anderson, 1992) (Figures 3B and 3C), suggesting that a portion of the EGFP$^+$ cells in the AGM region were NCSCs. At E12.5, most of the EGFP$^+$ cells were positive for tyrosine hydroxylase

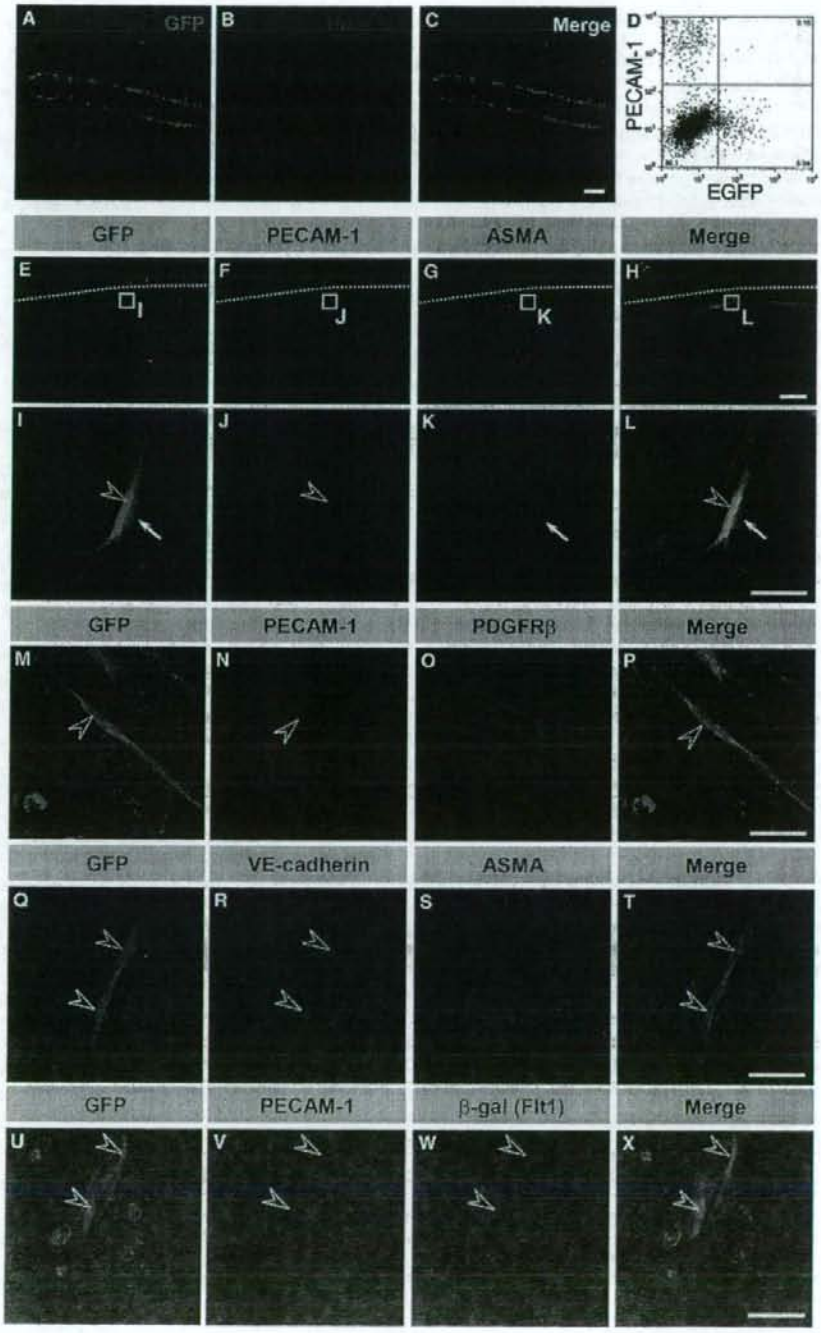
A
GFP
B
C
Merge
D
PECAM-1
EGFP
GFP
PECAM-1
ASMA
Merge
E
F
G
H
I
J
K
L
GFP
PECAM-1
PDGFRβ
Merge
M
N
O
P
GFP
VE-cadherin
ASMA
Merge
Q
R
S
T
GFP
PECAM-1
β-gal (Flt1)
Merge
U
V
W
X

(TH), a marker of catecholaminergic neurons that make up the para-aortic plexus (Figure 3D), raising the possibility that EGFP$^+$ Sox10$^-$ cells at E11.0 were neuroblasts that differentiated into TH$^+$ neurons at E12.5. However, the small number of TH$^-$ EGFP$^+$ cells that invaded the aorta were positive for p75 and Sox10 (Figures 3E–3H), suggesting that the cells entering the blood vessel were NCSCs. None of the EGFP$^+$ cells at the periphery of aorta were positive for GFAP (Figure 3I), ruling out the possibility that the EGFP$^+$ cells are newly arrived Schwann cells that are migrating along the vasculature. EGFP$^+$ p75$^+$ cells were also observed in peripheral blood at E12.5 by immunohistochemistry (Figures 3J and 3K), and flow-cytometric analysis of the blood taken from E13.5 to E15.5 mice detected EGFP$^+$ cells (Figure 3L). In E14.5 mice, immunohistochemistry revealed EGFP$^+$ Sox10$^+$ cells in the fetal liver (Figures 3M and 3N). After E18.5, no EGFP$^+$ cells were detected in the circulating blood (Figure 3L). Similar results were observed in the AGM region, peripheral blood, and fetal liver in Wnt1-Cre/Floxed-EGFP mice (Figure S3). These observations suggest that NCSCs migrate in the blood to the BM via the AGM region, specifically during E12.5–E15.5, similar to HSCs.

Sphere-Forming Capability of Neural Crest-Derived Cells from Adult Mice

To compare neural crest-derived cells from the DRG, WP, and BM, cells from these tissues were collected from postnatal 2-, 4-, 8-, and 13-week-old P0-Cre/Floxed-EGFP mice, and their EGFP expression was analyzed by flow cytometry. The frequency of EGFP$^+$ cells from each source was highest at 2 weeks of age and decreased over time (Figures 4A and 4B). The same result was observed in Wnt1-Cre/Floxed-EGFP mice (Figure S4A). Interestingly, the number of EGFP$^+$ cells collected from the BM increased when the bones were treated with collagenase. Since collagenase releases BM cells that adhere tightly to the bone (Funk et al., 1994), this suggests that the neural crest-derived cells observed histologically were tightly associated with the BM surface.

The formation of neurosphere-like spheres from neural crest-derived tissue has been reported (Fernandes et al., 2004; Tomita et al., 2005; Yoshida et al., 2006) using culture procedures similar to neurosphere-culture protocols for cells of the central nervous system (CNS) (Reynolds and Weiss, 1992). To confirm the capability of neural crest-derived cells to proliferate and form spheres, EGFP$^+$ and EGFP$^-$ cells from the DRG, WP, and BM of 8-week-old P0-Cre/Floxed-EGFP mice were collected by flow cytometry and cultured at a density of 5×10^3 cells/ml (Hulspas et al., 1997) in serum-free sphere-forming medium containing human epidermal growth factor (EGF), human fibroblast growth factor 2 (FGF2), and B27. The EGFP$^+$ cells proliferated to form spheres that were morphologically similar to CNS neurospheres after 14 days (Figure 4C). When cultured at the same density, the highest number of spheres was formed from cells derived from the DRG and the lowest from the BM (Figure 4D). Cultured EGFP$^-$ cells derived from the DRG and BM did not form spheres, but those from the WP did, albeit at a much lower frequency than the EGFP$^+$ cells (Figure 4D). Sphere-forming capacity and tissue-specific sphere-forming efficacy in cells from adult Wnt1-Cre/Floxed-EGFP mice were similar to those from P0-Cre/Floxed-EGFP mice (Figures S4B and S4C). These results indicate that neural crest-derived cells capable of proliferating into spheres exist in the adult DRG and BM in addition to the WP, which has been previously reported.

Spheres Derived from Each Adult Tissue Contain Multipotent NCSCs

Previous reports have characterized NCSCs by their ability to self-renew and their capacity for multilineage differentiation (multipotency) into neurons, glial cells, and myofibroblasts (Morrison et al., 1999; Shah et al., 1996). To evaluate the differentiation potential of EGFP$^+$ spheres generated from sorted EGFP$^+$ cells, we cultured EGFP$^+$ spheres from the three tissue sources of adult P0-Cre/Floxed-EGFP mice for 10 days in 10% serum-containing differentiation medium. The differentiated cells were identified by triple immunostaining: neurons by β-III tubulin, glial cells by glial fibrillary acidic protein (GFAP), and myofibroblasts by SMA. EGFP$^+$ spheres from all three sources demonstrated trilineage differentiation potential (Figure 5A), but the differentiation preference differed depending on the tissue source (Table 1). Most of the DRG-derived spheres showed trilineage differentiation potential (NGM, 74.6%), but the frequency was significantly lower in the WP- and BM-derived spheres (NGM, 7.3% and 3.3%, respectively). The WP-derived spheres displayed a bilineage differentiation tendency into neurons and myofibroblasts (NM, 91.6%), while most BM-derived spheres differentiated into myofibroblasts (M, 64.6%), suggesting that EGFP$^+$ cells derived from the WP and BM are mostly lineage-restricted progenitors, with only a small percentage possessing multilineage differentiation potential. In addition, when EGFP$^+$ DRG-derived spheres were cultured in differentiation medium containing 5-bromo-2′-deoxyuridine (BrdU) (Figure 5B), all three resulting cell types (N, M, and G) were positive for BrdU. Therefore, these three cell types from DRG-derived spheres probably originated from mitotic precursor cells within the

Figure 2. EGFP$^+$ Cells Contribute to Vascular Endothelial and Smooth Muscle Cells in the BM of P0-Cre/Floxed-EGFP Mice

(A–C) EGFP$^+$ cells were detected along vasculature in the tibia.

(D) Representative EGFP- and PECAM-1-gated flow-cytometric analysis chart. To prevent the contamination of macrophages, CD45$^+$ cells were removed before analysis.

(E–L) Triple immunohistochemistry for GFP, PECAM-1, and SMA in whole-mount specimens. Note the abundant EGFP$^+$ cells around the inner surface of the bone cortex (outer surface indicated by dotted lines). (I–L) High-magnification views of the boxed areas in (E)–(H), respectively. Note the EGFP$^+$ endothelial cells (arrowheads) and smooth muscle cells (arrows).

(M–P) Triple immunohistochemistry for GFP, PECAM-1, and PDGFRβ, a marker for pericytes and smooth muscle cells. The arrowhead indicates EGFP$^+$ PECAM-1$^+$ endothelial cells.

(Q–T) EGFP$^+$ cells were also positive for VE-cadherin, a marker for endothelial cells (arrowheads).

(U–X) In triple-transgenic mice encoding P0-Cre/Floxed-EGFP/Flt1^{lacZ}, EGFP$^+$ cells were positive for PECAM-1 and β-gal (arrowheads). Flt1 is expressed in endothelial and hematopoietic cells. Scale bars, 50 μm in (A)–(C), 200 μm in (E)–(H), and 20 μm in (I)–(X).

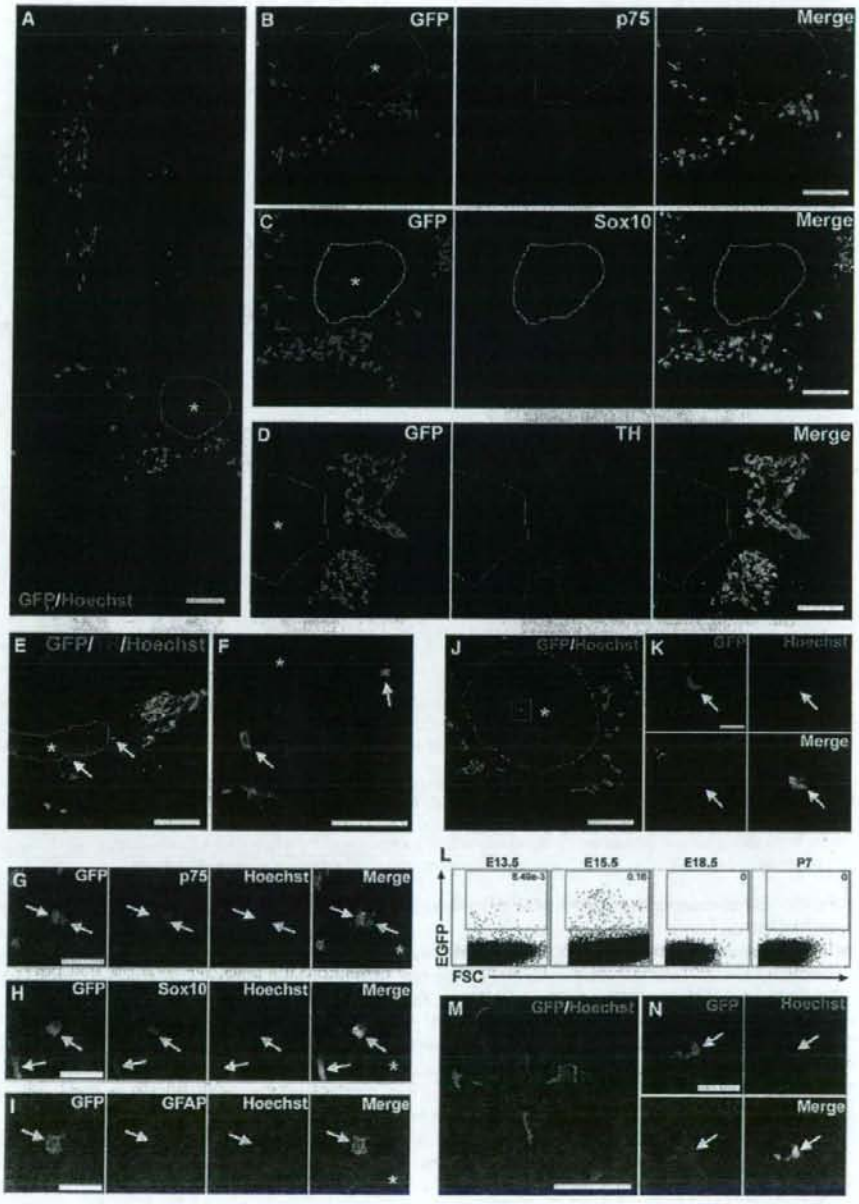

Figure 3. Histological Analyses of the AGM Region and Flow-Cytometric Analyses of Peripheral Blood in P0-Cre/Floxed-EGFP Mice

(A) At E11.0, EGFP$^+$ cells detected by anti-GFP antibodies were seen migrating from the dorsal neural tube into the AGM region. The region enclosed in a dashed line with an asterisk indicates the aorta.

(B and C) Double immunohistochemistry of the AGM region revealed that EGFP$^+$ cells were positive for p75 (B) and partially colocalized with Sox10 (C), indicating that EGFP$^+$ cells in the embryonic AGM region expressed NCSC markers.

(D–F) At E12.5, most EGFP$^+$ cells had differentiated into TH-positive catecholaminergic neurons (D), but some EGFP$^+$ TH$^-$ cells invaded the aorta (arrows in [E] and [F]).

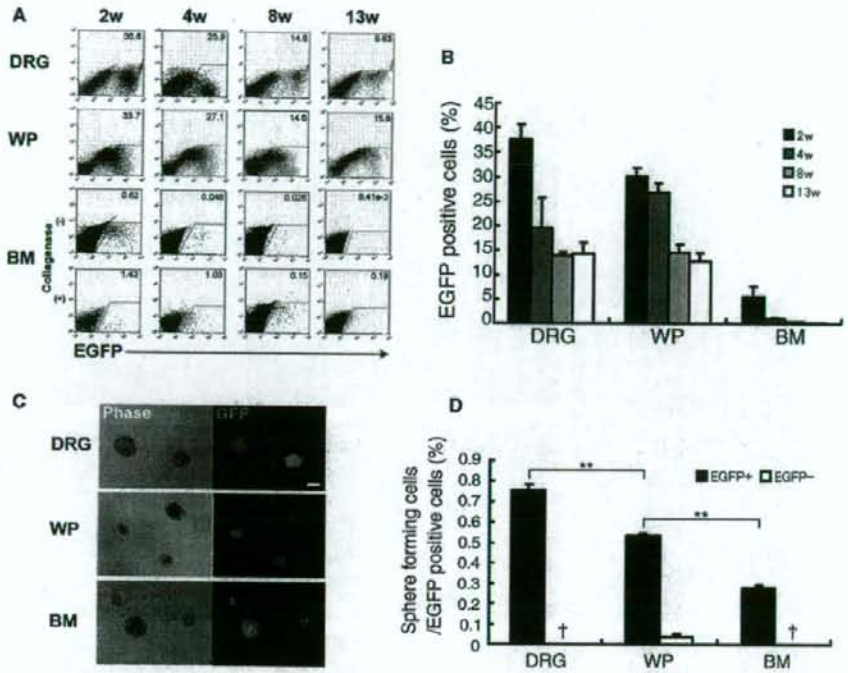

Figure 4. Isolation and Sphere-Forming Capacity of Neural Crest-Lineage Cells Derived from the DRG, WP, and BM in Adult P0-Cre/Floxed-EGFP Mice

(A) Representative EGFP-gated flow-cytometric analysis charts of cells from the DRG, WP, and BM of postnatal 2-, 4-, 8-, and 13-week-old mice. In the BM, the number of collected EGFP$^+$ cells increased with collagenase treatment.

(B) The number of collected EGFP$^+$ cells from all three sources decreased with age (mean ± SEM, n = 3 per group).

(C) Phase-contrast and direct EGFP-fluorescent images showing spheres formed from EGFP$^+$ cells after 14 days in culture. Scale bar, 50 μm.

(D) The percentage of sphere-forming cells found in each tissue source was assessed by culturing EGFP$^+$ and EGFP$^-$ cells from each source at a cell density of 5×10^3 cells/ml and counting the number of spheres formed (mean ± SEM; n = 3 per group; **p < 0.01; †, no sphere observed). The highest percentage of sphere-forming cells was observed in the DRG, and the WP was the only source with EGFP$^-$ cells capable of forming spheres.

spheres and did not represent contamination of postmitotic cells from the original tissue.

Recent reports have questioned the validity of "clonal density" cultures (Jessberger et al., 2007; Singec et al., 2006), demonstrating that CNS neurospheres are motile structures that can fuse even at cellular concentrations previously regarded as "clonal" (Hulspas et al., 1997). To assess the possible effects of sphere fusion in our culture protocol, we examined the differentiation of spheres cultured in medium containing 0.8% methylcellulose (Figures S5A–S5C). This method, which we previously reported (Yoshida et al., 2006), effectively prevents sphere fusion, resulting in spheres that are more than 90% clonal. Differentiation studies of these clonal spheres yielded results similar to those shown in Table 1 (Figure S5D), indicating that the influence of sphere fusion was quite limited. Results from adult Wnt1-Cre/Floxed-EGFP mice corroborated data from adult P0-Cre/Floxed-EGFP mice, revealing the formation of clonal spheres from the DRG, WP, and BM that possessed a similar differentiation preference (Figures S4B–S4E).

To assess the self-renewal capacity of the EGFP$^+$ spheres, secondary sphere-forming assays were conducted. EGFP$^+$ spheres derived from each tissue source of P0-Cre/Floxed-EGFP mice were independently placed into one well of a 96-well plate, dissociated into single cells, and cultured in sphere-forming medium. The frequency of secondary sphere formation was highest in cells derived from the DRG (Figure 5C), confirming that, of these three sources, the DRG contains the highest frequency of NCSCs.

(G–I) At E12.5, most EGFP$^+$ cells at the periphery of the aorta were positive for p75 and Sox10 but negative for GFAP.

(J and K) EGFP$^+$ p75$^+$ cells were observed in the peripheral blood of E12.5 mice (boxed area in [J] magnified in [K]).

(L) EGFP-gated flow-cytometric analysis charts of embryonic and postnatal blood cells. EGFP$^+$ cells were detected from E13.5 and E15.5, but not at E18.5 or after birth. Transverse axis indicates forward scatter (FSC).

(M and N) At E14.5, EGFP$^+$ cells were observed in the liver. Some were positive for Sox10, indicating that NCSCs exist in the liver. Scale bars, 100 μm in (A)–(F), (J), and (M); 50 μm in (G)–(I), and (N); and 20 μm in (K).

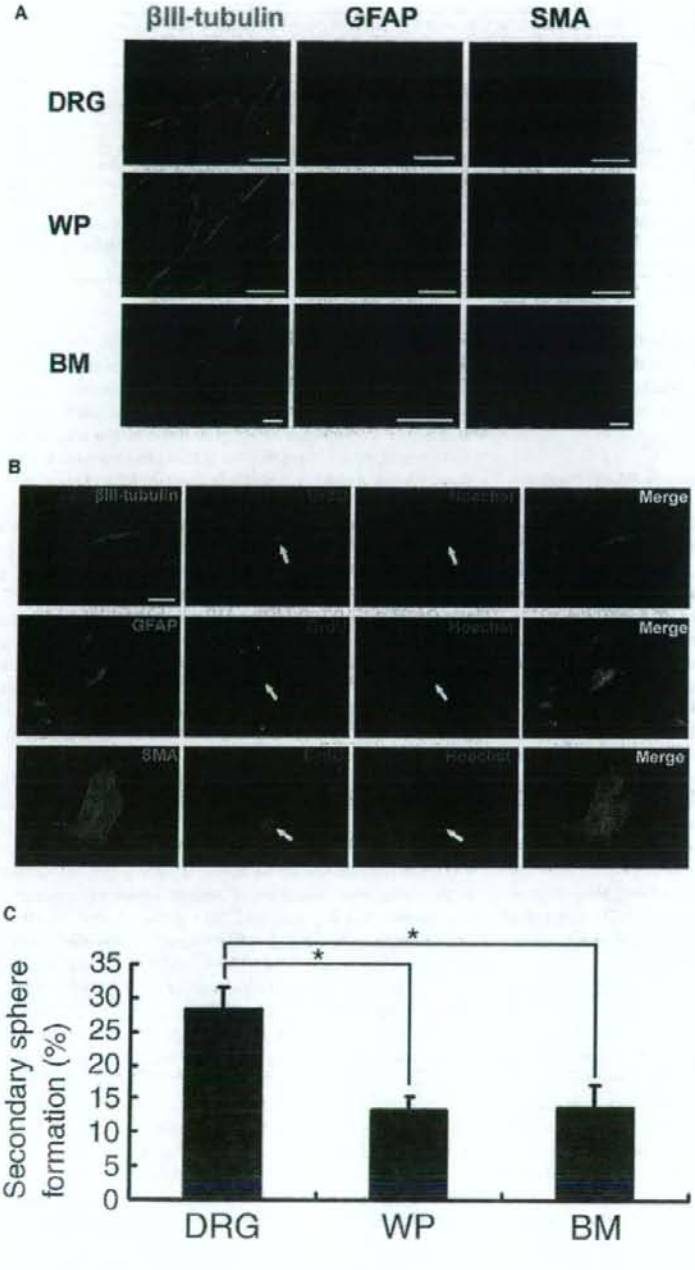

Figure 5. Differentiation and Secondary Sphere-Forming Capacity of EGFP⁺ Spheres Derived from the DRG, WP, and BM in Adult P0-Cre/Floxed-EGFP Mice

(A) EGFP⁺ spheres formed from each tissue source differentiated into neurons, glial cells, and myofibroblasts. Scale bars, 50 μm.

(B) DRG-derived spheres were cultured in medium containing BrdU. Cells double positive for BrdU and each cell-type-specific marker were observed. Scale bar, 25 μm.

(C) When these spheres were dissociated, the DRG-derived cells formed the greatest number of secondary spheres, indicating their high capacity for self-renewal (mean ± SEM; n = 3 per group; $^*p < 0.05$).

Expression Pattern of Neural Crest-Associated Genes Differs among Tissue Sources

To characterize the mRNA expression profile of neural crest cells derived from each tissue, cells from the adult P0-Cre/Floxed-EGFP mice were analyzed by semiquantitative RT-PCR for various markers, especially neural crest-associated genes (Figure 6A). The following were prepared from each adult tissue source: noncultured EGFP⁻ and EGFP⁺ cells, cultured spheres, and cells differentiated from spheres. The noncultured cells showed varying tissue-source-dependent gene expression patterns. EGFP⁺ cells from the DRG strongly expressed the known NCSC markers *Sox10* and *p75*. Although their expression of the neural crest markers *Snail*, *Slug*, *Twist*, *Sox9*, and *Pax3* was lower or undetectable compared to EGFP⁻ cells, most of these markers were expressed after culture. The expression of neural crest-associated genes was quite similar in EGFP⁺ and EGFP⁻ cells from the WP, whereas in the BM, their expression was significantly higher in EGFP⁺ cells compared to EGFP⁻ cells.

For the EGFP⁺ spheres, although the expression frequencies of neural crest-associated genes differed, the spheres from all three tissues generally expressed most of the neural crest-associated genes. By comparison, CNS neurospheres derived from the E14.5 striatum did not express the neural crest-associated genes *Snail*, *Slug*, *Twist*, *p75*, or *Pax3*. They expressed *sox9* and *sox10* as expected, since these genes are also deeply involved in development of the CNS (Stolt et al., 2003, 2004). *Nkx6.1* is a well-known marker expressed in the ventral half of the neural tube during early development (Jensen et al., 1996). EGFP⁺ cells and spheres did not express *Nkx6.1*, in contrast to its strong expression in embryonic stem cell-derived neurospheres ventralized by the sonic hedgehog protein (Shh)

Table 1. Differentiation Potential of Spheres Derived from DRG, WP, and BM of Adult P0-Cre/Floxed-EGFP Mice

Frequency of Sphere Types (Percent ± SD)								
	NGM	NM	NG	GM	N	M	G	Others
DRG	74.6 ± 1.0	21.8 ± 3.6	2.3 ± 3.2	0	1.0 ± 0.2	0	0	0
WP	7.3 ± 3.6	91.6 ± 3.1	0	0	0	1.1 ± 1.1	0	0
BM	3.3 ± 0.4	15.6 ± 0.8	0.5 ± 0.8	0.8 ± 0.7	7.3 ± 8.5	64.6 ± 11.7	0.7 ± 1.2	7.3 ± 2.6

EGFP$^+$ spheres formed from clonal density cultures of each tissue source were differentiated and subjected to triple immunostaining. The differentiation potential of 100 spheres from each tissue source was individually examined, and each sphere's ability to differentiate into each cell type was determined: N, neurons; G, glial cells; M, myofibroblasts (mean ± SD, n = 3 per group). Spheres derived from the DRG showed a significantly higher frequency of trilineage differentiation potential (N + G + M) than the spheres from other sources ($p < 0.05$ by Kruskal-Willis test). Of the spheres derived from the BM, 7.3% were negative for all three lineage markers.

(Y.O. and H.O., unpublished data). These results indirectly suggest that the examined cells did not have ventral identities and do not conflict with the fact that they are developmentally derived from the dorsal neural tube, where neural crest cells originate.

EGFP$^+$ Cells of the DRG Strongly Express NCSC Markers in Adult P0-Cre/Floxed-EGFP Mice

To quantify the expression of the NCSC markers *Sox10* and *p75* in fresh noncultured EGFP$^+$ cells and in spheres cultured for 2 weeks, we performed real-time PCR (Figure 6B). *Sox10* and *p75* expression was higher in both the noncultured cells and cultured spheres from the DRG compared with those from the WP and BM, suggesting that there is a higher proportion of NCSCs in the DRG. However, since these genes are also expressed in specific neurons and glial cells (Kaplan and Miller, 2000; Paratore et al., 2001), we examined the expression levels of *Nestin* and *Musashi1*. Although they are used as markers for undifferentiated cells in the CNS (Lendahl et al., 1990; Sakakibara et al., 1996), they are also expressed in neural crest-derived sphere initiating cells from the heart (Tomita et al., 2005), cornea (Yoshida et al., 2006) and gut (R. Hotta, S.S., and H.O., unpublished data). Since it has been suggested that *Nestin* and *Musashi1* expression may reflect an undifferentiated state (Tomita et al., 2005), their high expression in spheres generated from the DRG also suggests that the DRG contains the highest proportion of NCSCs, and their increased expression after culture suggests that these NCSCs proliferate in culture when spheres are formed.

DISCUSSION

In the present study, by using the double-transgenic mouse strains P0 and Wnt1-Cre/Floxed-EGFP, we examined multiple tissues and organs to map the presence of neural crest-derived cells. We discovered the existence of multipotent NCSCs in the BM and DRG of adult rodents along with the previously reported facial WP. However, analysis of these cells revealed interesting differences that were specific to the tissue source. Careful consideration of these differences will be necessary if these cells are to be recruited for cell transplantation treatments.

Our histological analysis of adult P0 and Wnt1-Cre/Floxed-EGFP mice revealed EGFP$^+$ cells in the BM (Figure 1 and Figure S1). Using flow cytometry, we collected EGFP$^+$ BM cells that proliferated to form spheres (Figure 4). Although the frequency was low, compared with the other tissue sources, multipotent NCSCs were present in the BM. Clonal spheres with a trilineage differentiation potential into neurons, glial cells, and myofibroblasts were observed, and dissociated cells from these spheres formed secondary spheres (Figure 5, Figures S4 and S5). The presence of NCSCs in the BM is also supported by a recent report using the same P0-Cre reporter mice to demonstrate that a portion of MSCs in the BM of the lower extremities are of neural crest lineage (Takashima et al., 2007). Furthermore, we have unpublished data showing that NCSCs contribute to produce a subpopulation of MSCs in the BM. At the embryonic stage, NCSCs differentiate into many types of neural crest lineage cells, most of which are marked with EGFP in P0 and Wnt1-Cre/Floxed-EGFP mice. We prospectively isolated EGFP$^+$ MSCs from the BM of P0 and Wnt1-Cre mice using flow cytometry and identified that EGFP$^+$ MSCs could generate osteocytes, chondrocytes, and adipocytes (S.M. and Y.M., unpublished data). Together with Nishikawa's report, these findings show that a certain population of MSCs in the BM originates from multipotent NCSCs.

Since a previous report indicated that Wnt1 is expressed in the BM of adult rodents (Almeida et al., 2005), we cannot rule out the possibility that the EGFP$^+$ labeling in the BM of adult Wnt1-Cre/Floxed-EGFP mice was due to the ongoing expression of Wnt1 in the adult BM rather than reflecting a history of Wnt1 expression in the embryonic neural crest lineage. However, we found that the sphere-forming potential and differentiation tendency of EGFP$^+$ cells from the BM of Wnt1-Cre/Floxed-EGFP mice were similar to those from P0-Cre/Floxed-EGFP mice (Figure S4), suggesting the presence of NCSCs among the EGFP$^+$ cells in the BM of adult Wnt1-Cre/Floxed-EGFP mice. The BM stem cells reported in other studies differentiated into neurons and glial cells in vitro and in vivo and also in transplantation experiments (Fernandez et al., 2004; Jiang et al., 2002). Although transdifferentiation or dedifferentiation has been suggested to explain this phenomenon, our results demonstrating the presence of NCSCs in the BM indicate that this differentiation potential may reflect that of NCSCs of the BM. It will be interesting to clarify the relationship between the NCSCs described in the present study and the BM-derived stem cells that are reported to generate neural cells in vitro (Kohyama et al., 2001).

Hematopoiesis is initiated in the yolk sac at the embryonic stage and is successively transferred to the AGM region, fetal liver, and BM with time (Dzierzak and Speck, 2008). Using two independent Cre lines, we detected NCSCs in the AGM region, fetal liver, and BM during a time frame that coincided with the

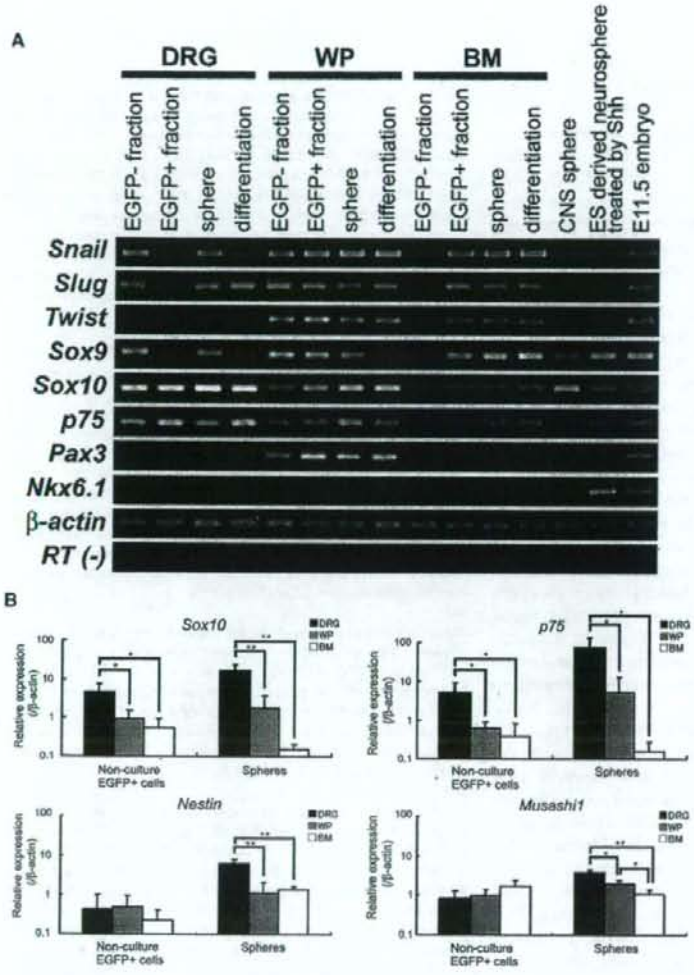

Figure 6. Expression Patterns of Embryonic Neural Crest-Specific Markers in Adult P0-Cre/Floxed-EGFP Mice

(A) Semiquantitative RT-PCR was conducted to evaluate the mRNA expression of various NCSC markers. Four types of cells were examined for each tissue source: EGFP$^-$ and EGFP$^+$ cells freshly fractionated by flow cytometry, EGFP$^+$ spheres after 14 days in culture, and differentiated cells. Total RNA from a whole E11.5 embryo was collected as a positive control. The expression frequencies of neural crest-lineage markers from the three tissue sources were variable and quite different from the CNS-type neurospheres cultured from the striatum of an E14.5 mouse (CNS sphere). The ventral marker *Nkx6.1*, observed in ES-cell-derived neurospheres ventralized by Shh induction, was not observed in any of the EGFP$^+$ neural crest-derived spheres.

(B) Quantitative PCR analysis revealed significantly higher expression of the NCSC markers *Sox10* and *p75* in the cells derived from the adult DRG. Immature stem/progenitor specific markers *Nestin* and *Musashi1* were also highly expressed in the DRG-derived spheres. $^*p < 0.05$, $^{**}p < 0.01$.

adult mice. Compared with the cells derived from the WP and BM, the neural crest-derived cells of the DRG contained a higher proportion of tripotent cells and displayed a greater ability to form secondary spheres (Figure 5 and Table 1). The expression levels of the NCSC markers *Sox10* and *p75*, and markers for undifferentiated stem/progenitor cells, *Nestin* and *Musashi1*, were also higher in the DRG-derived EGFP$^+$ cells from adult P0-Cre/Floxed-EGFP mice (Figure 6B), suggesting that the DRG contained the highest proportion of NCSCs of the tissues studied. The origin of the NCSCs in the DRG is presently unknown. The DRG develops from two sources: neural crest cells that follow the ventromedial pathway and BC cells that originate from the dorsal root entry zone (Maro et al., 2004). BC cells are also neural crest-derived populations that transiently occupy the dorsal entry and ventral exit points of trunk spinal nerve roots during peripheral nervous system development (Altman and Bayer, 1984; Niederlander and Lumsden, 1996). Since embryonic BC cells include multipotent NCSCs (Hjerling-Leffler et al., 2005), it is possible that NCSCs originating from the BC migrate to and remain in the DRG until adulthood.

The presence of NCSCs in the facial skin and whisker follicle was reported previously (Fernandes et al., 2004; Sieber-Blum et al., 2004), and our results confirm their existence. An interesting finding was the formation of spheres from EGFP$^-$ cells of the WP of P0 and Wnt1-Cre/Floxed-EGFP mice, although at a significantly lower percentage than the EGFP$^+$ cells (Figure 4D and

period of hematopoiesis of each site, suggesting that NCSCs join the migration pathway of hematopoietic cells on the way to the BM from the embryonic period through adulthood. Our present findings concerning the migration stream of NCSCs imply an undiscovered relationship between NCSCs and hematopoiesis.

The DRG is derived from the neural crest. Although several groups have demonstrated the existence of NCSCs in the embryonic DRG (Laimeroth et al., 2002; Paratore et al., 2001), we confirmed their existence in the DRG of adult rodents. Recently, DRG-derived sphere-initiating cells were reported in adult rodents, but their origin and potential were not elucidated (Li et al., 2007). In our present study, using P0 and Wnt1-Cre reporter mice, we demonstrated that the observed cells were of neural crest lineage. Furthermore, examination of the spheres formed through a valid clonal culture method confirmed the presence of cells with stem cell-like properties in the DRG of

Figure S4C). These EGFP$^-$ spheres may develop from stem/progenitor cells with an origin other than the neural crest, such as the keratinocyte stem cells of the epithelium (Kobayashi et al., 1993). However, since the gene expression profile of EGFP$^-$ cells was similar to that of EGFP$^+$ cells, this seems unlikely (Figure 6A). Another possible explanation for their presence is transgene silencing through epigenetic modifications such as DNA methylation, which can weaken EGFP expression (Turker, 2002). When EGFP$^-$ spheres were cultured in medium containing the demethylating agent 5-azacytidine, we observed EGFP expression in some of them (data not shown), suggesting that DNA methylation-mediated transgene silencing partially accounts for the presence of EGFP$^-$ spheres.

Our results from culturing and characterizing NCSCs from the adult BM, DRG, and WP revealed significant tissue-source-dependent differences. Similarly, NCSCs from the embryonic gut and sciatic nerve exhibit heritable, cell-intrinsic differences in their responses to lineage-determination factors in vitro and in vivo (Bixby et al., 2002). Factors that come into play during the segregation, migration, and maintenance of neural crest cells have been proposed to explain these differences in NCSC characteristics. In the premigratory neural tube, a gradient of multiple signals is present along the rostrocaudal neuraxis, affecting the premigratory neural crest cells (Abzhanov et al., 2003; Lwigale et al., 2004). Once the neural crest cells separate from the neural tube, they are exposed to a multitude of factors through their path of migration, and NCSCs that survive in each respective tissue are affected by factors within that tissue (Couly et al., 2002; Trainor et al., 2002). There are also differences between embryonic and postnatal stages, as revealed in a study showing differences between fetal and adult gut NCSCs (Kruger et al., 2002). Therefore, it may be unrealistic to attempt to characterize NCSCs as a single population, since those from different sources display different traits. Instead, it will be important to understand these differences and to elucidate the molecular mechanisms for the maintenance and lineage determination of NCSCs in each tissue.

NCSCs are attracting increasing interest as potential candidates for cell transplantation therapy of nerve trauma and disease, because they are present in tissue that can be harvested from the patient. This allows for autologous transplantation, avoiding immunological complications as well as the ethical concerns associated with embryonic stem cells. We isolated and examined NCSCs from adult tissues with this in mind and discovered that NCSCs from different tissues had distinct characteristics. Further study of these NCSCs will hopefully lead to the culture and transplantation of NCSCs most appropriate for the lesion receiving treatment.

EXPERIMENTAL PROCEDURES

Animals

Transgenic mice expressing Cre recombinase under control of the P0 promoter (P0-Cre) (Yamauchi et al., 1999) and Wnt1 promoter/enhancer (Wnt1-Cre) (Danielian et al., 1998) were mated with EGFP reporter mice (CAG-CAT$^{loxP/loxP}$-EGFP) (Kawamoto et al., 2000) to obtain P0-Cre/Floxed-EGFP and Wnt1-Cre/Floxed-EGFP double-transgenic mice. Mice heterozygous for a null allele of Flt1 (Flt1$^{+/lacZ}$) (Fong et al., 1995) were crossed to P0-Cre/Floxed-EGFP double-transgenic mice to obtain P0-Cre/Floxed-EGFP/Flt1^{lacZ} triple transgenic mice. Adult wild-type mice were purchased for mating from CLEA Japan. All experimental procedures were approved by the ethics committee of Keio University and were in accordance with the Guide for the Care and Use of Laboratory Animals (U.S. National Institutes of Health).

Immunohistochemistry

For histological analysis, samples were fixed in 4% paraformaldehyde (PFA) and embedded in cryomold for sectioning at 14 μm. The following antibodies were used as primary antibodies: anti-green fluorescent protein (GFP) (rabbit IgG, 1:500, MBL, and goat IgG, 1:200, Santa Cruz Biotechnology), Sox10 (goat IgG, 1:200, R&D Systems), p75 (rabbit IgG, 1:500, Chemicon), TH (sheep IgG, 1:200, Chemicon), and P0 (chick IgG, 1:200, Aves). Immunoreactivity was visualized using secondary antibodies conjugated with Alexa 488 or Alexa 568 (Molecular Probes). Nuclear counterstaining was performed with Hoechst 33342 (10 μg /ml, Sigma B2261). The samples were observed with a confocal laser scanning microscope (LSM510, Carl Zeiss). Whole-mount preparation of tibias and immunostaining were performed as described (Kubota et al., 2008).

Preparation of DRG, WP, and BM Cells

Juvenile (14–28 days) and adult (2–12 months) P0-Cre/Floxed-EGFP mice were deeply anesthetized and sacrificed by cervical dislocation.

DRG

The vertebral body was dissected out, and the DRGs from C5 to L5 were resected into HBSS$^+$ (GIBCO 14025-092) supplemented with 10% fetal bovine serum (FBS; Equitech-Bio SFB30-1478) and 1% penicillin/streptomycin (P/S; GIBCO-BRL). The peripheral nerve tissue was removed, and the DRGs were incubated with 0.25% collagenase (Sigma C5894) in HBSS$^+$ for 30 min at 37°C. After being rinsed in PBS, the DRGs were incubated in 0.25% trypsin-EDTA for 30 min at 37°C and mechanically dissociated into DRG medium (neurobasal medium [GIBCO 21103-049] supplemented with 20 ng/ml B27 [GIBCO], 1% L-glucose [GIBCO], and 1% P/S). The cells were collected by centrifugation at 800 × g for 3 min at 4°C.

WP

The facial WP was carefully dissected, washed in HBSS, and incubated in 0.3% dispase II (Roche 1276921) in DMEM-F12 (GIBCO 11330-032) containing 1% P/S for 3 hr at 37°C. Hair and dermis were removed with a cell lifter (Costar). The skin tissue was minced into small pieces and digested with 0.04% collagenase (Wako 038-10531) in DMEM-F12 for 1 hr at 37°C. Cell clusters were mechanically dissociated in medium, and the suspension was poured through a 70 μm cell strainer (Falcon). The dissociated cells were collected by centrifugation at 480 × g for 3 min at 4°C.

BM

The femurs and tibias were dissected out and crushed with a pestle. The crushed bones were washed in HBSS$^+$ (GIBCO 14175-095) supplemented with 2% FBS, 10 mM HEPES (GIBCO 15630-080), and 1% P/S to remove hematopoietic cells. The bone fragments were collected and incubated for 1 hr at 37°C in 0.2% collagenase (Wako 032-10534) in DMEM (GIBCO 11885-084) containing 10 mM HEPES and 1% P/S. The suspension was filtered with a cell strainer (Falcon 2350) and collected by centrifugation at 280 × g for 7 min at 4°C. The pellet was resuspended for 5–10 s in 1 ml water (Sigma W3500) to burst red blood cells, after which 1 ml of 2 × PBS (diluted from Sigma D1408) containing 4% FBS was added. The cells were resuspended in HBSS$^-$, and the suspension was poured through a cell strainer.

Flow-Cytometric Analysis

Flow-cytometric analysis was performed as described previously (Matsuzaki et al., 2004). For detailed analysis of the BM in P0-Cre/Floxed-EGFP mice, BM cells were stained for 30 min on ice with PE-anti-PECAM-1 and APC-anti-CD45 (eBioscience, CA). After collecting 1 × 10^6 events, the fluorescence intensity of PECAM-1 and EGFP in the CD45-negative cell population was plotted as a two-dimensional dot plot.

Blood cells from embryos were obtained by cutting the umbilical arteries and allowing the blood to flow freely into PBS. After collecting the PBS, EGFP$^+$ cells were identified by EGFP fluorescence.

Primary and Secondary Sphere-Forming Cultures

Cells from the DRG, WP, and BM were seeded at 5 × 10^3 cells/ml (Hulspas et al., 1997) in a serum-free sphere-forming medium consisting of DMEM/F-12 (1:1) (GIBCO 12100-046/21700-075) supplemented with insulin (25 μg/ml), transferrin (100 μg/ml), progesterone (20 nM), sodium selenate

(30 nM), putrescine (60 nM) (all from Sigma-Aldrich), recombinant human EGF (100 ng/ml) (Pepro Tech #100-15), human FGF-basic (100 ng/ml) (Pepro Tech #100-18b), and B27 (20 ng/ml) (modified from Reynolds and Weiss [1992]). Cells were cultured in an incubator at 37°C, 5% CO_2, and half of the medium was changed every 6–7 days. For BrdU labeling, 1 μM BrdU was added to the culture medium every 3 days. For clonal sphere expansion, the cells were cultured in the above medium with 0.8% methylcellulose (nacalai tesque 22224-55) (Yoshida et al., 2006).

For secondary sphere formation assays, primary spheres were collected, incubated in 0.25% trypsin-EDTA for 30 min at 37°C, and triturated until a single-cell suspension was obtained. The cells were spun at 860 × g for 3 min at 4°C and resuspended in the aforementioned sphere culture medium.

For statistical evaluation of the primary and secondary sphere-forming assays, one-factor ANOVA and the Tukey-Kramer test were applied.

Differentiation Analysis

Spheres were plated on poly-D-lysin/laminin (Sigma P7405/Invitrogen 23017-015)-coated 8-well chamber slides (Iwaki 5732-008) and cultured for 10 days in the following differentiation medium: DMEM/F12 (1:1) supplemented with 10% FBS, without any growth factors. For immunocytochemistry, the cells were fixed in 4% PFA and stained with the following primary antibodies: anti-GFAP (rabbit IgG, 1:500, Dako Z0334), β-III tubulin (mouse IgG2b, 1:500, Sigma T8660), αSMA (mouse IgG2a, 1:1000, Sigma A2547), and BrdU (sheep IgG, 1:500, Fitzgerald 20-BS17). Secondary antibodies were the following: anti-mouse IgG2b (Alexa 488 A-21141), anti-mouse IgG2a (Alexa 350 A-21130), anti-rabbit IgG (Alexa 568 A11036), and anti-sheep IgG (Alexa 568 A-21099 [1:1000, Molecular Probes]). The samples were observed with a universal fluorescence microscope (Axioskop 2 Plus; Carl Zeiss).

RT-PCR Assay

RT-PCR assay is described in the Supplemental Experimental Procedures. For statistical analysis, real-time RT-PCR results were evaluated using Student's t test.

SUPPLEMENTAL DATA

Supplemental Data include five figures, Supplemental Experimental Procedures, and Supplemental References and can be found with this article online at http://www.cellstemcell.com/cgi/content/full/2/4/392/DC1/.

ACKNOWLEDGMENTS

We thank H.J. Okano, K. Takubo, R. Hotta, K. Ando, and Y. Muguruma for helpful discussions; S. Shimmura, S. Yoshida, I. Hamaguchi, T. Mizukami, and S. Miyao for technical support; and T. Harada for tender animal care. We also thank Janet Rossant, Department of Molecular and Medical Genetics, University of Toronto, for generously providing $Flt1^{+/lacZ}$ mice. This work was supported by grants from the Leading Project for the Realization of Regenerative Medicine from the Ministry of Education, Culture, Sports, Science and Technology (MEXT), Japan; the General Insurance Association of Japan; and a Grant-in-Aid for the 21st century COE program from MEXT to Keio University. The authors declare that they have no competing financial interests.

Received: May 8, 2007
Revised: November 12, 2007
Accepted: March 11, 2008
Published: April 9, 2008

REFERENCES

Abzhanov, A., Tzahor, E., Lassar, A.B., and Tabin, C.J. (2003). Dissimilar regulation of cell differentiation in mesencephalic (cranial) and sacral (trunk) neural crest cells in vitro. Development *130*, 4567–4579.

Almeida, M., Han, L., Bellido, T., Manolagas, S.C., and Kousteni, S. (2005). Wnt proteins prevent apoptosis of both uncommitted osteoblast progenitors and differentiated osteoblasts by beta-catenin-dependent and -independent signaling cascades involving Src/ERK and phosphatidylinositol 3-kinase/AKT. J. Biol. Chem. *280*, 41342–41351.

Altman, J., and Bayer, S.A. (1984). The development of the rat spinal cord. Adv. Anat. Embryol. Cell Biol. *85*, 1–164.

Bhattacharyya, A., Frank, E., Ratner, N., and Brackenbury, R. (1991). P0 is an early marker of the Schwann cell lineage in chickens. Neuron *7*, 831–844.

Bixby, S., Kruger, G.M., Mosher, J.T., Joseph, N.M., and Morrison, S.J. (2002). Cell-intrinsic differences between stem cells from different regions of the peripheral nervous system regulate the generation of neural diversity. Neuron *35*, 643–656.

Couly, G., Creuzet, S., Bennaceur, S., Vincent, C., and Le Douarin, N.M. (2002). Interactions between Hox-negative cephalic neural crest cells and the foregut endoderm in patterning the facial skeleton in the vertebrate head. Development *129*, 1061–1073.

Danielian, P.S., Muccino, D., Rowitch, D.H., Michael, S.K., and McMahon, A.P. (1998). Modification of gene activity in mouse embryos in utero by a tamoxifen-inducible form of Cre recombinase. Curr. Biol. *8*, 1323–1326.

D'Ippolito, G., Diabira, S., Howard, G.A., Menei, P., Roos, B.A., and Schiller, P.C. (2004). Marrow-isolated adult multilineage inducible (MIAMI) cells, a unique population of postnatal young and old human cells with extensive expansion and differentiation potential. J. Cell Sci. *117*, 2971–2981.

Dzierzak, E., and Speck, N.A. (2008). Of lineage and legacy: the development of mammalian hematopoietic stem cells. Nat. Immunol. *9*, 129–136.

Etchevers, H.C., Vincent, C., Le Douarin, N.M., and Couly, G.F. (2001). The cephalic neural crest provides pericytes and smooth muscle cells to all blood vessels of the face and forebrain. Development *128*, 1059–1068.

Fernandes, K.J., McKenzie, I.A., Mill, P., Smith, K.M., Akhavan, M., Barnabe-Heider, F., Biernaskie, J., Junek, A., Kobayashi, N.R., Toma, J.G., et al. (2004). A dermal niche for multipotent adult skin-derived precursor cells. Nat. Cell Biol. *6*, 1082–1093.

Fernandez, C.I., Alberti, E., Mendoza, Y., Martinez, L., Collazo, J., Rosillo, J.C., and Bauza, J.Y. (2004). Motor and cognitive recovery induced by bone marrow stem cells grafted to striatum and hippocampus of impaired aged rats: functional and therapeutic considerations. Ann. N Y Acad. Sci. *1019*, 48–52.

Fong, G.H., Rossant, J., Gertsenstein, M., and Breitman, M.L. (1995). Role of the Flt-1 receptor tyrosine kinase in regulating the assembly of vascular endothelium. Nature *376*, 66–70.

Funk, P.E., Kincade, P.W., and Witte, P.L. (1994). Native associations of early hematopoietic stem cells and stromal cells isolated in bone marrow cell aggregates. Blood *83*, 361–369.

Hjerling-Leffler, J., Marmigere, F., Heglind, M., Cederberg, A., Koltzenburg, M., Enerback, S., and Ernfors, P. (2005). The boundary cap: a source of neural crest stem cells that generate multiple sensory neuron subtypes. Development *132*, 2623–2632.

Hulspas, R., Tiarks, C., Reilly, J., Hsieh, C.C., Recht, L., and Quesenberry, P.J. (1997). In vitro cell density-dependent clonal growth of EGF-responsive murine neural progenitor cells under serum-free conditions. Exp. Neurol. *148*, 147–156.

Jensen, J., Serup, P., Karlsen, C., Nielsen, T.F., and Madsen, O.D. (1996). mRNA profiling of rat islet tumors reveals nkx 6.1 as a beta-cell-specific homeodomain transcription factor. J. Biol. Chem. *271*, 18749–18758.

Jessberger, S., Clemenson, G.D., Jr., and Gage, F.H. (2007). Spontaneous fusion and nonclonal growth of adult neural stem cells. Stem Cells *25*, 871–874.

Jiang, Y., Jahagirdar, B.N., Reinhardt, R.L., Schwartz, R.E., Keene, C.D., Ortiz-Gonzalez, X.R., Reyes, M., Lenvik, T., Lund, T., Blackstad, M., et al. (2002). Pluripotency of mesenchymal stem cells derived from adult marrow. Nature *418*, 41–49.

Joseph, N.M., Mukouyama, Y.S., Mosher, J.T., Jaegle, M., Crone, S.A., Dormand, E.L., Lee, K.F., Meijer, D., Anderson, D.J., and Morrison, S.J. (2004). Neural crest stem cells undergo multilineage differentiation in developing peripheral nerves to generate endoneurial fibroblasts in addition to Schwann cells. Development *131*, 5599–5612.

Kaplan, D.R., and Miller, F.D. (2000). Neurotrophin signal transduction in the nervous system. Curr. Opin. Neurobiol. *10*, 381–391.

Kawamoto, S., Niwa, H., Tashiro, F., Sano, S., Kondoh, G., Takeda, J., Tabayashi, K., and Miyazaki, J. (2000). A novel reporter mouse strain that expresses enhanced green fluorescent protein upon Cre-mediated recombination. FEBS Lett. *470*, 263–268.

Kobayashi, K., Rochat, A., and Barrandon, Y. (1993). Segregation of keratinocyte colony-forming cells in the bulge of the rat vibrissa. Proc. Natl. Acad. Sci. USA *90*, 7391–7395.

Kohyama, J., Abe, H., Shimazaki, T., Koizumi, A., Nakashima, K., Gojo, S., Taga, T., Okano, H., Hata, J., and Umezawa, A. (2001). Brain from bone: efficient "meta-differentiation" of marrow stroma-derived mature osteoblasts to neurons with Noggin or a demethylating agent. Differentiation *68*, 235–244.

Kruger, G.M., Mosher, J.T., Bixby, S., Joseph, N., Iwashita, T., and Morrison, S.J. (2002). Neural crest stem cells persist in the adult gut but undergo changes in self-renewal, neuronal subtype potential, and factor responsiveness. Neuron *35*, 657–669.

Kubota, Y., Takubo, K., and Suda, T. (2008). Bone marrow long label-retaining cells reside in the sinusoidal hypoxic niche. Biochem. Biophys. Res. Commun. *366*, 335–339.

Le Douarin, N.M., and Kalcheim, C. (1999). The neural crest (Cambridge: Cambridge University Press).

Leimeroth, R., Lobsiger, C., Lussi, A., Taylor, V., Suter, U., and Sommer, L. (2002). Membrane-bound neuregulin1 type III actively promotes Schwann cell differentiation of multipotent Progenitor cells. Dev. Biol. *246*, 245–258.

Lemke, G., Lamar, E., and Patterson, J. (1988). Isolation and analysis of the gene encoding peripheral myelin protein zero. Neuron *1*, 73–83.

Lendahl, U., Zimmerman, L.B., and McKay, R.D. (1990). CNS stem cells express a new class of intermediate filament protein. Cell *60*, 585–595.

Li, H.Y., Say, E.H., and Zhou, X.F. (2007). Isolation and characterization of neural crest progenitors from adult dorsal root ganglia. Stem Cells *25*, 2053–2065.

Lwigale, P.Y., Conrad, G.W., and Bronner-Fraser, M. (2004). Graded potential of neural crest to form cornea, sensory neurons and cartilage along the rostrocaudal axis. Development *131*, 1979–1991.

Maro, G.S., Vermeren, M., Voiculescu, O., Melton, L., Cohen, J., Charnay, P., and Topilko, P. (2004). Neural crest boundary cap cells constitute a source of neuronal and glial cells of the PNS. Nat. Neurosci. *7*, 930–938.

Matsuzaki, Y., Kinjo, K., Mulligan, R.C., and Okano, H. (2004). Unexpectedly efficient homing capacity of purified murine hematopoietic stem cells. Immunity *20*, 87–93.

Medvinsky, A., and Dzierzak, E. (1996). Definitive hematopoiesis is autonomously initiated by the AGM region. Cell *86*, 897–906.

Mendes, S.C., Robin, C., and Dzierzak, E. (2005). Mesenchymal progenitor cells localize within hematopoietic sites throughout ontogeny. Development *132*, 1127–1136.

Morrison, S.J., White, P.M., Zock, C., and Anderson, D.J. (1999). Prospective identification, isolation by flow cytometry, and in vivo self-renewal of multipotent mammalian neural crest stem cells. Cell *96*, 737–749.

Muller, A.M., Medvinsky, A., Strouboulis, J., Grosveld, F., and Dzierzak, E. (1994). Development of hematopoietic stem cell activity in the mouse embryo. Immunity *1*, 291–301.

Niederlander, C., and Lumsden, A. (1996). Late emigrating neural crest cells migrate specifically to the exit points of cranial branchiomotor nerves. Development *122*, 2367–2374.

Paratore, C., Goerich, D.E., Suter, U., Wegner, M., and Sommer, L. (2001). Survival and glial fate acquisition of neural crest cells are regulated by an interplay between the transcription factor Sox10 and extrinsic combinatorial signaling. Development *128*, 3949–3961.

Reynolds, B.A., and Weiss, S. (1992). Generation of neurons and astrocytes from isolated cells of the adult mammalian central nervous system. Science *255*, 1707–1710.

Ross, J.J., Hong, Z., Willenbring, B., Zeng, L., Isenberg, B., Lee, E.H., Reyes, M., Keirstead, S.A., Weir, E.K., Tranquillo, R.T., et al. (2006). Cytokine-induced differentiation of multipotent adult progenitor cells into functional smooth muscle cells. J. Clin. Invest. *116*, 3139–3149.

Sakakibara, S., Imai, T., Hamaguchi, K., Okabe, M., Aruga, J., Nakajima, K., Yasutomi, D., Nagata, T., Kurihara, Y., Uesugi, S., et al. (1996). Mouse-Musashi-1, a neural RNA-binding protein highly enriched in the mammalian CNS stem cell. Dev. Biol. *176*, 230–242.

Shah, N.M., Groves, A.K., and Anderson, D.J. (1996). Alternative neural crest cell fates are instructively promoted by TGFbeta superfamily members. Cell *85*, 331–343.

Sieber-Blum, M., Grim, M., Hu, Y.F., and Szeder, V. (2004). Pluripotent neural crest stem cells in the adult hair follicle. Dev. Dyn. *231*, 258–269.

Singec, I., Knoth, R., Meyer, R.P., Maciaczyk, J., Volk, B., Nikkhah, G., Frotscher, M., and Snyder, E.Y. (2006). Defining the actual sensitivity and specificity of the neurosphere assay in stem cell biology. Nat. Methods *3*, 801–806.

Stemple, D.L., and Anderson, D.J. (1992). Isolation of a stem cell for neurons and glia from the mammalian neural crest. Cell *71*, 973–985.

Stolt, C.C., Lommes, P., Sock, E., Chaboissier, M.C., Schedl, A., and Wegner, M. (2003). The Sox9 transcription factor determines glial fate choice in the developing spinal cord. Genes Dev. *17*, 1677–1689.

Stolt, C.C., Lommes, P., Friedrich, R.P., and Wegner, M. (2004). Transcription factors Sox8 and Sox10 perform non-equivalent roles during oligodendrocyte development despite functional redundancy. Development *131*, 2349–2358.

Takashima, Y., Era, T., Nakao, K., Kondo, S., Kasuga, M., Smith, A.G., and Nishikawa, S. (2007). Neuroepithelial cells supply an initial transient wave of MSC differentiation. Cell *129*, 1377–1388.

Tomita, Y., Matsumura, K., Wakamatsu, Y., Matsuzaki, Y., Shibuya, I., Kawaguchi, H., Ieda, M., Kanakubo, S., Shimazaki, T., Ogawa, S., et al. (2005). Cardiac neural crest cells contribute to the dormant multipotent stem cell in the mammalian heart. J. Cell Biol. *170*, 1135–1146.

Trainor, P.A., Ariza-McNaughton, L., and Krumlauf, R. (2002). Role of the isthmus and FGFs in resolving the paradox of neural crest plasticity and prepatterning. Science *295*, 1288–1291.

Turker, M.S. (2002). Gene silencing in mammalian cells and the spread of DNA methylation. Oncogene *21*, 5388–5393.

Wong, C.E., Paratore, C., Dours-Zimmermann, M.T., Rochat, A., Pietri, T., Suter, U., Zimmermann, D.R., Dufour, S., Thiery, J.P., Meijer, D., et al. (2006). Neural crest-derived cells with stem cell features can be traced back to multiple lineages in the adult skin. J. Cell Biol. *175*, 1005–1015.

Yamauchi, Y., Abe, K., Mantani, A., Hitoshi, Y., Suzuki, M., Osuzu, F., Kuratani, S., and Yamamura, K. (1999). A novel transgenic technique that allows specific marking of the neural crest cell lineage in mice. Dev. Biol. *212*, 191–203.

Yoshida, S., Shimmura, S., Nagoshi, N., Fukuda, K., Matsuzaki, Y., Okano, H., and Tsubota, K. (2006). Isolation of multipotent neural crest-derived stem cells from the adult mouse cornea. Stem Cells *24*, 2714–2722.

Isolation and characterization of dendritic cells from common marmosets for preclinical cell therapy studies

Shigeki Ohta,[1] Yoko Ueda,[2] Masae Yaguchi,[1] Yumi Matsuzaki,[3] Masaya Nakamura,[4] Yoshiaki Toyama,[4] Yoshikuni Tanioka,[5] Norikazu Tamaoki,[5] Tatsuji Nomura,[5] Hideyuki Okano,[3] Yutaka Kawakami[2] and Masahiro Toda[1,6]

[1]*Neuroimmunology Research Group, Keio University School of Medicine, Tokyo,* [2]*Division of Cellular Signaling, Institute for Advanced Medical Research, Keio University School of Medicine, Tokyo,* [3]*Department of Physiology, Keio University School of Medicine, Tokyo,* [4]*Department of Orthopaedic Surgery, Keio University School of Medicine, Tokyo,* [5]*Central Institute for Experimental Animals, Kawasaki, Kanagawa, and* [6]*Department of Neurosurgery, Keio University School of Medicine, Tokyo, Japan*

doi:10.1111/j.1365-2567.2007.02727.x
Received 9 February 2007; revised 16 July 2007; accepted 29 August 2007.
Correspondence: Masahiro Toda, Neuroimmunology Research Group and Department of Neurosurgery, Keio University School of Medicine, 35 Shinanomachi, Shinjuku-ku, Tokyo 160-8582, Japan.
Email: todam@sc.itc.keio.ac.jp
Senior author: Shigeki Ohta, email: shiohta@sc.itc.keio.ac.jp

Summary

Dendritic cells (DCs) have important functions as modulators of immune responses, and their ability to activate T cells is of great value in cancer immunotherapy. The isolation of DCs from the peripheral blood of rhesus and African green monkeys has been reported, but the immune system in the common marmoset remains poorly characterized, although it offers many potential advantages for preclinical studies. In the present study, we devised methods, based on techniques developed for mouse and human DC preparation, for isolating DCs from three major tissue sources in the common marmoset: bone marrow (BM), spleen and peripheral blood. Each set of separated cells was analysed using the cell surface DC-associated markers CD11c, CD80, CD83, CD86 and human leucocyte antigen (HLA)-DR, all of which are antibodies against human antigens, and the cells were further characterized both functionally and morphologically as antigen-presenting cells. BM proved to be an excellent cell source for the isolation of DCs intended for preclinical studies on cell therapy, for which large quantities of cells are required. In the BM-derived $CD11c^+$ cell population, cells exhibiting the characteristic features of DCs were enriched, with the typical DC morphology and the abilities to undergo endocytosis, to secrete interleukin (IL)-12, and to stimulate Xenogenic T cells. Moreover, BM-derived DCs produced the neurotrophic factor NT-3, which is also found in murine splenic DCs. These results suggest that BM-derived DCs from the common marmoset may be useful for biological analysis and for preclinical studies on cell therapy for central nervous system diseases and cancer.

Keywords: antigen-presenting cells; primate; dendritic cells; NT-3

Introduction

Dendritic cells (DCs) have the ability to prime T cells to produce immune responses against viruses, bacteria and tumours. When immature, DCs can capture and process exogenous antigens; following maturation, they enhance the expression of both major histocompatibility complex (MHC) class II and costimulatory molecules, and migrate to lymphoid organs, where they stimulate potent antigen-specific T cells.[1,2] Because of their high ability to activate cytotoxic T lymphocytes, DCs are regarded as a useful tool in cancer immunotherapy and are currently being used in human clinical studies.[3–6] Furthermore, we reported a new use of DCs for the treatment of central nervous system (CNS) diseases such as spinal cord injury (SCI), involving the activation of endogenous neural stem/progenitor cells (NSPCs).[7]

DCs have been extensively characterized in humans and rodents. The use of primates, instead of rodents, to examine the therapeutic effects of DC therapy is an important step towards future clinical studies on the treatment of SCI and cancer. Although DCs have been isolated from rhesus and African green monkeys,[8–12] the characteristics of DCs and other components of the immune system of the common marmoset (CM) remain unclear. Therefore, methods for the isolation of DCs from the CM and the

subsequent characterization of these cells are needed for preclinical studies.

Compared with other monkeys, the CM offers many advantages for preclinical studies.[13,14] The average weight of an adult CM is between 200 and 300 g, making it possible to handle and breed them easily on a large scale and reducing the cost of experiments.[14] Sequence analysis of the entire CM genome is progressing at Washington University and the National Institutes of Health (NIH) Intramural Sequencing Center, and the results of these efforts will clarify the genetic similarity between the CM and humans. Because of these advantages, CMs have been widely used in many studies involving gene therapy,[15,16] bacterial infection,[17] toxicology[18] and immunology.[19,20] The usefulness of a CM model for studies on CNS diseases has also been shown for Parkinson's disease,[21] stroke,[22] Huntington disease,[23] multiple sclerosis,[24,25] anxiety[26] and SCI.[27,28] In addition, human antibodies have been reported to be cross-reactive to CM peripheral blood cells,[29,30] and a CM anti-CD34 antibody has been produced for studying haematopoietic cells.[31,32] In this study, we established methods for isolating DCs from the bone marrow (BM), spleen and peripheral blood mononuclear cells (PBMC) of the CM; all of these tissues contain DC progenitor cells. Furthermore, in view of the excellent yield of DCs from BM, we focused on the characterization of these cells for use in preclinical studies on cell therapy.

Materials and methods

Animals

Healthy CMs (body weight 200–350 g; age 1–8 years) were selected from experimental stock at the Central Institute for Experimental Animals (Kawasaki, Japan) and were killed for isolation of DCs from tissues, as described below. All animal experiments were performed according to the guidelines of the Animal Care and Use Committee of the Keio University School of Medicine.

Antibodies

The cross-reactivities of the following fluorescein isothiocyanate (FITC)-, phycoerythrin (PE)- or allophycocyamin (APC)-conjugated anti-human monoclonal antibodies (mAbs) to CM were determined by flow cytometry and were found to agree with previous results:[15,29,30] CD1a (clone HI149; eBioscience, San Diego, CA), CD1c (clone AD5-8E7; MiltenyiBiotec, Bergisch Gladbach, Germany; clone 11·86; Becton Dickinson, San Jose, CA), CD3 (clone SP34; BD Pharmingen, San Diego, CA), CD4 (clone MT310; DAKO Cytomation, Glostrup, Denmark), CD8 (clone T8; Beckman Coulter, Miami, FL), CD11c (clone S-HCL-3; Becton Dickinson), CD14 (clone TUK4; DAKO Cytomation; clone M5E2; BD Pharmingen), CD34 (clone BIRMA-K3; DAKO Cytomation), CD80 (clone MAB104; Beckman Coulter), CD83 (clone HB15a; Beckman Coulter), CD86 (clone B-T7; Diaclone, Besançon, France), and HLA-DR (clone G46-6; BD Pharmingen).

Isolation of DCs from BM cells

Femurs and tibias were removed and left in 70% ethanol for a few minutes before washing in phosphate-buffered saline (PBS). Both ends were cut with scissors, and the marrow was flushed with RPMI-1640 (Sigma, St Louis, MO) using a plastic pipette. Cluster cells were dissociated by vigorous pipetting and were filtered through a cell strainer (100 μm; BD Falcon, Billerica, MA). Red blood cells were removed using an ACK lysis buffer (BioWhittaker, Walkersville, MD). BM cells were suspended in RPMI-1640 supplemented with 10% heat-inactivated fetal calf serum (FCS) at a cell density of 2×10^7 cells/ml and were cultured at 37° in 5% CO_2. After overnight incubation, suspension cells were collected, adjusted to a cell density of 4×10^5 cells/ml, and plated on six-well plates (Costar Corp., Cambridge, MA) in a complete medium (cRPMI), which consisted of RPMI-1640 supplemented with 10% FCS, penicillin and streptomycin (50 U/ml; Invitrogen, Carlsbad, CA), recombinant human granulocyte–macrophage colony-stimulating factor (rhGM-CSF) (100 ng/ml; PeproTech, Rocky Hill, NJ), and recombinant human interleukin-4 (rhIL-4) (100 ng/ml; PeproTech), based on the method for generating mouse BM-derived DCs.[33,34] The reactivity of human GM-CSF and IL-4 on CM cells has been previously demonstrated.[35,36] Half the supernatant was replenished with fresh cRPMI on culture day 4, and the floating cells were collected as a DC-enriched cell fraction on culture day 7 or 8. In this study, DCs were also generated from $CD34^+$ BM progenitor cells based on methods previously reported.[9,11] Sorted $CD34^+$ BM cells were plated RPMI-1640 medium supplemented with 10% FCS, 1% non-essential amino acids (Invitrogen), 1 mM sodium pyruvate, 10 mM HEPES, rhGM-CSF (100 ng/ml), penicillin and streptomycin (50 U/ml; Invitrogen), recombinant human Flt-3 ligand (rhFlt-3 ligand) (100 ng/ml; PeproTech), recombinant human stem cell factor (rhSCF) (100 ng/ml; PeproTech), and tumour necrosis factor-α (rhTNF-α) (5 ng/ml; PeproTech). On culture day 2, the same amounts of cytokines were added again to the medium. On day 5, cells were recultured in cRPMI supplemented with hrTNF-α (5 ng/ml), and further cultured for 1 week. For maturation, the BM cell culture was stimulated with 1 μg/ml *Escherichia coli* (055:B5)-derived lipopolysaccharide (LPS; Sigma) for 24 hr. To enrich the $CD11c^+$ cell population, the floating cultured cells were labelled with PE-conjugated anti-human CD11c mAb and directly purified by cell sorting on Moflo (DAKO Cytomation) or further labelled with anti-PE immunomagnetic beads (Milteny Biotec, Bergisch Gladbach, Germany) for cell sorting on AutoMACS (Milteny Biotec).

Isolation of DCs from spleen

Splenocytes were dissociated with Type IV collagenase (1 mg/ml; Sigma) in Hanks' balanced salt solution (HBSS) for 20 min at 37° and filtered out with a cell strainer (100-μm pores; BD Falcon) after cell homogenization. These cells were suspended in a dense bovine serum albumin (BSA) solution ($\rho = 1{\cdot}080$), overlaid with an equal volume of RPMI-1640 medium, and centrifuged in a swing bucket rotor at 9500 *g* for 15 min at 4°. The interface cell fraction was collected and analysed for cell surface antigens by flow cytometry. Splenic $CD11c^+$ cells were further sorted using either AutoMACS or Moflo as described above. For maturation, the $CD11c^+$ sorted cells were further incubated with LPS (1 μg/ml) in RPMI-1640 containing 10% FCS at 37° for 24 hr. These experiments were repeated at least five times.

Isolation of monocyte-derived DCs

PBMC were isolated from heparinized venous blood from CMs by gradient centrifugation using Lymphoprep ($\rho = 1{\cdot}077$; Nycomed, Oslo, Norway). Using anti-human CD14 mAb, the monocytes were purified by Moflo and cultured in cRMPI at a cell density of 5×10^5 cells/ml in a 48-well plate (Costar Corp) for 7 days. For maturation, the 7-day culture was stimulated with LPS (1 μg/ml) and interferon (IFN)-γ (100 ng/ml) for another 24 hr. These experiments were repeated at least five times.

Flow cytometric analysis

Cells ($1–5 \times 10^5$) were stained with the above-mentioned mAbs in PBS supplemented with 0·5% BSA for 30 min at room temperature and washed with PBS. A flow cytometric analysis was performed using an EPICS XL (Beckman Coulter, Miami, FL) or a FACS Calibur (BD Biosciences, San Jose, CA). Results are given as the percentage positive minus the background from appropriate isotype controls. Representative findings from several independent experiments were used.

Analysis of the xenogeneic mixed leucocyte reaction (MLR)

Adult human T cells were purified from PBMC using a magnetic microbeads separation kit [MACS human Pan T-cell isolation Kit; Miltenyi Biotec] as responder cells. In this study, xenogeneic human T cells were used because of difficulties in obtaining enough allogeneic CM T cells, referring to O'Doherty's work.[8] These responder cells (6×10^4) were seeded into a 96-well plate (Costar Corp.) together with titrated numbers of irradiated DCs as stimulators in 200 μl of RPMI-1640 supplemented with 10% human AB serum. After 5 days of coculturing, the cells were pulsed with 10 mM 5-bromo-2′ deoxyuridine (BrdU) for 24 hr and subjected to a BrdU incorporation assay using a cell proliferation enzyme-linked immunosorbent assay (ELISA) BrdU kit (Roche, Nutley, NJ) to measure newly synthesized DNA. Briefly, the cells were dried (2 hr at 60°), fixed in 70% ethanol in HCl (0·5 N) for 30 min at −20°, and incubated with peroxidase-conjugated mouse anti-BrdU mAb (30 min at room temperature). The reaction of the luminal substrate was measured using a luminometer (ARVO mx/Light Luminescence counter; PerkinElmer Life Sciences, Wellesley, MA). These experiments were repeated three times.

ELISA analysis

In the MLR experiments, the supernatants (day 2) were analysed for human IFN-γ (Endogene, Rockford, IL) and IL-4 (eBioscience, San Diego, CA) using the ELISA kits. The culture supernatants of the CM DCs stimulated with either LPS (1 μg/ml) or LPS (1 μg/ml) and IFN-γ (100 ng/ml, PeproTech) for 24 hr were analysed for IL-12 (p70) using an ELISA kit (R & D Systems, Minneapolis, MN). Lysates of BM-derived DCs and spleen tissue were assayed for neurotrophic factor NT-3 and brain-derived neurotrophic factor (BDNF) using an ELISA kit (Emax Immuno Assay System; Promega, Madison, WI). These experiments were repeated three times.

Analysis of endocytotic activity

The endocytotic activity of the DCs was measured as described previously.[33] BM-derived $CD11c^+$ cells were incubated with dextran-FITC (1 mg/ml; Sigma) at either 4° or 37° for 30 min in cRPMI. After washing in PBS, the cells were analysed using a FACS Calibur. For the immunocytochemical analysis, PE-labelled $CD11c^+$ cells were incubated with dextran-FITC (1 mg/ml; Sigma) at either 37° or 4° for 2 hr.

Immunocytochemical analysis

Cells were fixed in 4% paraformaldehyde in PBS for 20 min at room temperature and incubated with PE-conjugated anti-CD11c mAb and FITC-conjugated anti-HLA-DR mAb in antigen dilution solution (DAKO Cytomation) for 2 hr at 37° followed by counterstaining with 4′-6-diamidino-2-phenylindole (DAPI). Images were obtained using a confocal scanning laser microscope (LMS510; Carl Zeiss, Tokyo, Japan).

Statistical analysis

All statistical analyses were performed using the Student *t*-test.

Results

Generation of BM-derived DCs

BM cells were cultured in the presence of rhGM-CSF and rhIL-4. On day 7, 2–5% of the non-adherent cultured BM cells (non-adherent BM) were $CD11c^+$ $HLA\text{-}DR^+$, indicating that more than 1×10^7 of the $CD11c^+$ $HLA\text{-}DR^+$ cells were isolated from the CM specimen (Fig. 1a). More $CD11c^+$ $HLA\text{-}DR^+$ cells were generated in the presence of rhGM-CSF and rhIL-4 than in the presence of rhGM-CSF alone (data not shown). Although we also generated DCs from $CD34^+$ BM cells, the number of $CD11c^+$ $HLA\text{-}DR^+$ cells generated from $CD34^+$ BM cells was less than one-eighth of that from non-adherent BM cells. We then examined the change in phenotype of the $CD11c^+$ cells generated from non-adherent BM and $CD34^+$ BM cells following maturation with LPS stimulation. As shown in Fig. 1(a), with both methods, the LPS-stimulated $CD11c^+$ cells showed a higher expression of CD80, CD83, CD86 and HLA-DR than the non-stimulated $CD11c^+$ cells and these $CD11c^+$ cells from non-adherent BM cells and $CD34^+$ BM cells showed a similar expression pattern. Although approximately 20% of the non-stimulated $CD11c^+$ $HLA\text{-}DR^+$ gated cell population from non-adherent BM cells expressed CD14, these cells expressed CD1a (78%) and CD1c (93%), which are known as human DC markers,[37,38] but did not contain a $CD3^+$ population (Fig. 1b). Therefore, we generated DCs from non-adherent BM cells for further analyses.

Confocal imaging showed the colocalization of CD11c and HLA-DR on the surface of cells with numerous dendrites, a morphological characteristic of DCs (Fig. 1c). To examine the functional characteristics of BM-derived CM DCs, cytokine production, the ability to stimulate Xenogenic human T cells, and endocytotic activity were analysed. As shown in Figs 1(d) and 2, the LPS-stimulated $CD11c^+$ cells secreted IL-12 and caused a proliferation of Xenogenic human T cells in a dose-dependent fashion, indicating their potency as antigen-presenting cells. The BM-derived $CD11c^+$ cells incubated at 37° incorporated more dextran-FITC than the cells incubated at 4°, and the LPS-stimulated $CD11c^+$ cells (mature type) showed a lower endocytotic capacity than the non-stimulated $CD11c^+$ cells (immature type), consistent with the functional features of DCs (Fig. 3). Furthermore, an ELISA analysis revealed that human T cells cocultured with the LPS-stimulated $CD11c^+$ cells secreted IFN-γ but not IL-4, suggesting that BM-derived $CD11c^+$ cells in CMs could induce T helper type 1 (Th1) immune responses similar to those induced by human DC1 (Fig. 4). Taken together, the results from the phenotypic and functional analyses suggest that BM-derived $CD11c^+$ $HLA\text{-}DR^+$ cells have the characteristic features of DCs.

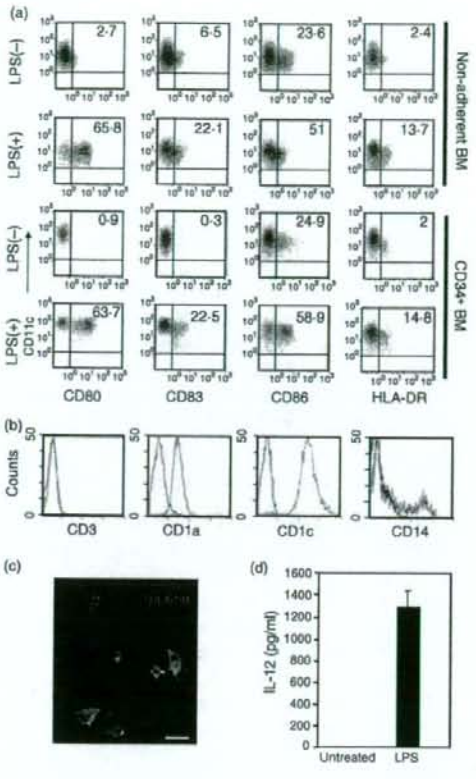

Figure 1. Characterization of bone marrow (BM)-derived dendritic cells (DCs) from common marmosets (CMs). (a) Expression of CD80, CD83, CD86 and human leucocyte antigen (HLA)-DR in $CD11c^+$ cells generated from non-adherent cultured BM cells (non-adherent BM) and $CD34^+$ BM cells on day 7 in culture. For maturation, cultured BM cells were treated with lipopolysaccharide (LPS; 1 μg/ml) for another 24 hr. The numbers within the dot blots represent the percentages within the quadrant. (b) Expression of $CD3^+$, CD1a, CD1c and CD14 in non-stimulated, non-adherent BM-derived $CD11c^+$ $HLA\text{-}DR^+$ cells (red line). Isotype controls are shown by a blue line. (c) Immunocytochemical analysis of BM-derived DCs. After stimulation with LPS for 24 hr, CD11c (red) and HLA-DR (green) were expressed on the cell surface of the dendrites. Scale bar, 10 μm. (d) Culture supernatants of BM-derived DCs treated with LPS for 24 hr were analysed for interleukin (IL)-12 using an enzyme-linked immunosorbent assay (ELISA).

Isolation of splenic DCs

After the splenocytes had been dissociated, a low density cell fraction was collected by centrifugation with dense BSA, based on a method used to isolate mouse splenic DCs.[39,40] For the CM specimens, $2–4 \times 10^5$ $CD11c^+$ cells were isolated from 1×10^7 of the BSA fractioned cells. As shown in Fig. 5(a), the $CD11c^+$ $CD8^+$ population was present in the CM spleen; this cell population is found

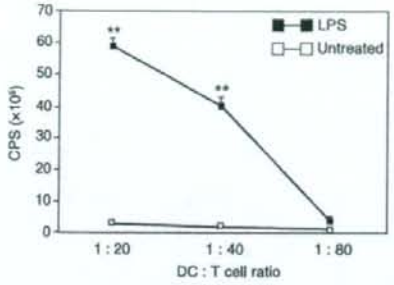

Figure 2. Mature bone marrow (BM)-derived dendritic cells (DCs) from common marmosets (CMs) stimulated the proliferation of xenogeneic human pan T cells. BM-derived $CD11c^+$ cells with or without lipopolysaccharide (LPS) stimulation (1 μg/ml) were cocultured at the indicated ratio with xenogeneic human pan-T cells (6×10^4) for 5 days. A 5-bromo-2′ deoxyuridine (BrdU) incorporation assay showed that the BM-derived $CD11c^+$ cells treated with LPS induced higher proliferation of Xenogenic T cells than the untreated BM-derived $CD11c^+$ cells. The $CD11c^+$ $HLA\text{-}DR^+$ cells constituted approximately 2% of the untreated $CD11c^+$ cell fraction and 14% of the LPS-treated $CD11c^+$ cell fraction, respectively. The mean ± standard deviation for duplicate wells is shown. $^{**}P < 0.01$. CPS, counts per second.

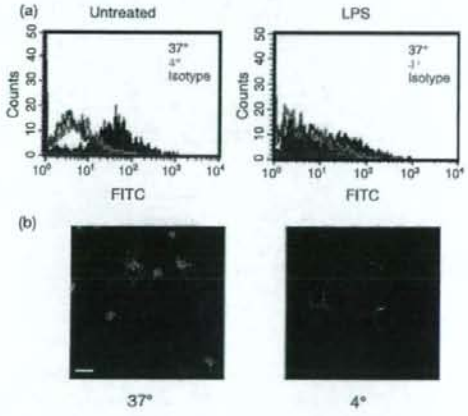

Figure 3. Immature bone marrow (BM)-derived dendritic cells (DCs) exhibit endocytotic activity. (a) BM-derived $CD11c^+$ cells stimulated with lipopolysaccharide (LPS; 1 μg/ml) or left untreated were incubated with dextran-fluorescein isothiocyanate (FITC) for 30 min at either 37° (shaded blue histograms) or 4° (green line) as a control for background passive uptake. The red line shows an isotype control. (b) Immature BM-derived DCs labelled with a phycoerythrin (PE)-conjugated anti-CD11c monocolonal antibody (mAb) were incubated with dextran-FITC at 37° or 4° for 2 hr. Confocal microscopy imaging showed fluorescent microspheres (green) in the cytoplasm of immature BM-derived $CD11c^+$ cells (red) incubated at 37°, but not in cells incubated at 4°. Scale bar, 10 μm.

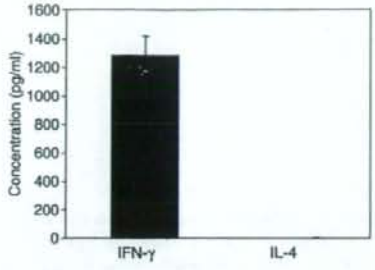

Figure 4. Interferon (INF)-γ secretion from human T cells in a xenogeneic mixed leucocyte reaction (MLR). The supernatants (2 days) of human pan T cells (6×10^4 cells/well) cocultured with irradiated lipopolysaccharide (LPS)-treated bone marrow (BM)-derived $CD11c^+$ cells (3×10^3 cells/well) were assayed for INF-γ and interleukin (IL)-4 using an enzyme-linked immunosorbent assay (ELISA). Data are shown as the mean ± standard deviation.

in mouse DCs. In mouse splenic DCs, the number of $CD11c^+$ $CD4^+$ DCs is approximately 2–3 times that of $CD11c^+$ $CD8^+$ DCs.[41,42] In contrast, the number of $CD11c^+$ $CD8^+$ cells was similar to the number of $CD11c^+$ $CD4^+$ cells in the CM spleen (Fig. 5a). The $CD11c^+$ $CD4^+$ cell population has been identified in human splenic DCs,[43] whereas the cells of the monocyte/macrophage lineage also express CD11c and CD4. Therefore, $CD11c^+$ $CD4^+$ cells in the CM spleen may contain some monocytes/macrophages. In the splenic $CD11c^+$ cells, the expression of HLA-DR and CD86 was increased by LPS stimulation (Fig. 5b). Upon LPS stimulation, the splenic $CD11c^+$ cells secreted higher amounts of IL-12 than the untreated $CD11c^+$ cells (Fig. 5c). The MLR analysis revealed that these $CD11c^+$ cells treated with LPS induced a stronger effect on the proliferation of xenogeneic human T cells (Fig. 6). Thus, the splenic $CD11c^+$ cells exhibited the functional features of DCs.

Generation of monocyte-derived DCs

Approximately 5×10^5 of the $CD14^+$ monocyte cells, less than 5% of the PBMC, were isolated from 10 to 15 ml of CM peripheral blood and were cultured in cRPMI including rhGM-CSF and rhIL-4 for 7 days. Although the yield depended on the individual CM specimens and approximately 20% of the cultured cells still expressed $CD14^+$, $1–2 \times 10^5$ $CD11c^+$ $HLA\text{-}DR^+$ cells showing the morphological characteristics of DCs were generated from one CM (data not shown). In monocyte-derived $CD11c^+$ cells, the expression of both HLA-DR and CD86 was increased by LPS and IFN-γ costimulation (Fig. 7a). IL-12 was also secreted from these cultured cells after stimulation with LPS and IFN-γ (Fig. 7b). Moreover, these monocyte-derived cells stimulated the

